2011

Multi-sensor Optimization Of The Simultaneous Turning And Boring Operation

Erick Johan Deane
University of Central Florida

MULTI-SENSOR OPTIMIZATION OF THE SIMULTANEOUS TURNING AND BORING OPERATION

by

ERICK JOHAN DEANE
B.S. University of Central Florida, 2010

A thesis submitted in partial fulfillment of the requirements
for the degree of Master of Science
in the Department of Mechanical, Materials, and Aerospace Engineering
in the College of Engineering and Computer Science
at the University of Central Florida
Orlando, Florida

Fall Term
2011

ABSTRACT

To remain competitive in today's demanding economy, there is an increasing demand for improved productivity and scrap reduction in manufacturing. Traditional manufacturing metal removal processes such as turning and boring are still one of the most used techniques for fabricating metal products. Although the essential metal removal process is the same, new advances in technology have led to improvements in the monitoring of the process allowing for reduction of power consumption, tool wear, and total cost of production. Replacing used CNC lathes from the 1980's in a manufacturing facility may prove costly, thus finding a method to modernize the lathes is vital.

This research focuses on Phase I and II of a three phase research project where the final goal is to optimize the simultaneous turning and boring operation of a CNC Lathe. From the optimization results it will be possible to build an adaptive controller that will produce parts rapidly while minimizing tool wear and machinist interaction with the lathe. Phase I of the project was geared towards selecting the sensors that were to be used to monitor the operation and designing a program with an architecture that would allow for simultaneous data collection from the selected sensors at high sampling rates. Signals monitored during the operation included force, temperature, vibration, sound, acoustic emissions, power, and metalworking fluid flow rates. Phase II of this research is focused on using the Response Surface Method to build empirical models for various responses and to optimize the simultaneous cutting process. The simultaneous turning and boring process was defined by the four factors of spindle speed, feed rate, outer diameter depth of cut, and inner diameter depth of cut. A total of four sets of experiments were performed. The first set of experiments screened the experimental region to

determine if the cutting parameters were feasible. The next three set s of designs of experiments used Central Composite Designs to build empirical models of each desired response in terms of the four factors and to optimize the process. Each design of experiments was compared with one another to validate that the results achieved were accurate within the experimental region.

By using the Response Surface Method optimal machining parameter settings were achieved. The algorithm used to search for optimal process parameter settings was the desirability function. By applying the results from this research to the manufacturing facility, they will achieve reduction in power consumption, reduction in production time, and decrease in the total cost of each part.

ACKNOWLEDGEMENTS

First of all I would like to thank my advisor, Dr. Chengying Xu for providing me with the challenge of leading this project. Under Dr. Xu's guidance we were able to meet the goals of the project in a timely manner. I would also like to thank Andrew Joslin for giving me the initial guidance and skills to successfully achieve the goals of the project. I would also like to thank the members of the GD team including Manuel Hernandez, Matthew Meanor, David Geiscke, and Schadrick Collins for all of their contributions to this research.

I would like to recognize Dr. Tony Schmitz from the University of Florida for his advice and contributions to this project. His contributions to the areas of tool wear, tool life, and chatter led us to several breakthroughs in this research.

This project would not have been possible without the help and funding from Dr. Dean Bartles from General Dynamics. I would like to thank him and his team including Glenn Groff and Keith Brown from the Red Lion facility. I would also like to thank Don Wilson from Breakthrough Management Group for his consulting on the use of design of experiments. In the design of experiments aspect, I would also like to thank my Response Surface Methodology professor Dr. Linda Malone from the University of Central Florida Industrial Engineering department.

Finally I would like to thank my family for their support and motivation to complete this research.

TABLE OF CONTENTS

LIST OF FIGURES

LIST OF TABLES

1 CHAPTER 1 - INTRODUCTION

1.1 Purpose and Motivation

Today's improvements in manufacturing technology have allowed for faster production and minimization of waste. One of the major improvements in the metal removal area of manufacturing has been the implementation of multi-axis machines. Multi-axis machines allow for simultaneous processing thus cutting the production times significantly. Although this is an outstanding achievement, very little is known about the complex interactions that occur in simultaneous machining.

Understanding of the simultaneous machining may prove difficult to model by analytical models which do not take into account the variability of the system. The variability of the system is further increased when the work pieces used have been forged and exposed to long periods of environmental exposure causing rust layers to form on the surface of the work piece. To truly understand the variability of the system an experimental approach such as a well-planned design of experiments may lead to accurate modeling of the system.

This research focuses on an ongoing three phase project for General Dynamics in which an Okuma LC-40 2ST CNC Lathe is used to understand the simultaneous turning and boring roughing operation of AISI 4137 chrome alloy steel. The roughing operation of a metal product takes a heavier toll on the lathe as it is the operation where most of the metal is removed. The first phase of the project focused mainly on sensor selection and sensor implementation. A vast amount of sensors are used in order to understand the machining process by measuring force,

power, vibration, temperature, tool wear, metal working fluid flow rate, hardness, etc. The main focus of the results of this research is set on the second phase. Phase II of this research applies a common statistical method known as Response Surface Methodology in order to build empirical models for the sensor responses and to optimize the machining operation. The third and final phase of this project will focus on using the results of Phase II in order to build an adaptive control system that will run the machine at optimal settings thus maximizing tool life and minimizing the cost.

General Dynamics produces the AISI 4137 chrome alloy steel work pieces at their Red Lion facility in Pennsylvania. The work pieces are first forged to their initial shape and then are machined by a CNC lathe to their final configuration. The forging process leaves two diameters on the work pieces which are known as the outer diameter (OD) and the inner diameter (ID). A drawing of a forged work piece can be seen in Figure 1-1.

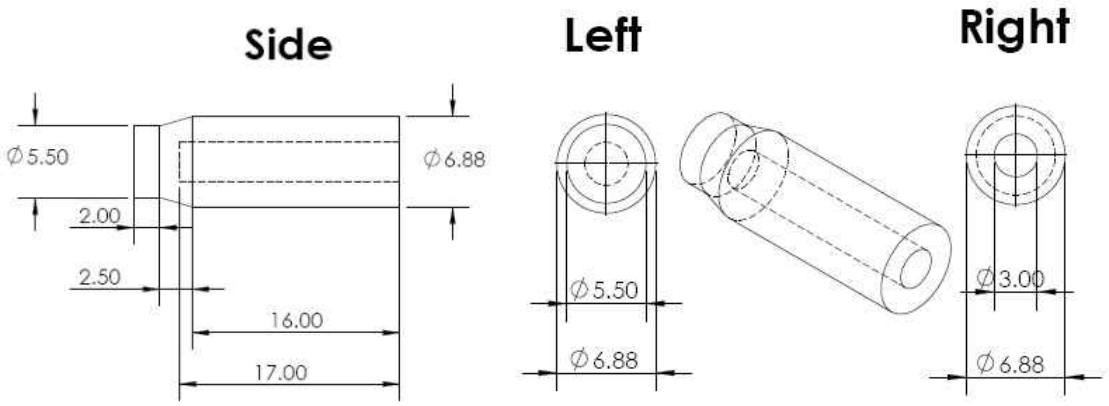

Figure 1-1: Drawing of AISI 4137 forged work piece (in.)

The forging process causes several defects in these parts such as imperfect diameters, ID eccentricity, and hardness variation. Also environmental effects come into account when parts sit outside the facility for months before machining, thus causing rust layers to form on the surface of the work pieces. When machining the work pieces two sets of passes are done on the work piece in order to reach the final configuration. The first pass is known as the roughing pass and the second is known as the finishing pass. The roughing pass uses heavy material removal tools to remove most of the excess material and the finishing pass uses finishing tools to adjust the work piece to its final specification of shape and surface roughness.

The roughing pass is the most critical machining process performed by the lathe. The consumption of resources by the roughing pass places the heaviest toll on the machine because of the heavy material removal and having to overcome the imperfections caused by the forging of the work piece. For this reasons this pass is the main focus of the optimization. During the roughing pass all of the nuisance factors introduced by forging and environmental effects cause undesired conditions in machining. These conditions include the chatter phenomena where the natural frequency of the system is excited and uncontrolled vibration of the system occurs. Another condition that has been experienced at the Red Lion facility is rapid tool failure caused by abnormal surfaces on the machining pass.

1.2 Outline

As mentioned in section 1.1 the focus of this research is based off using the Response Surface Methodology approach to optimizing the simultaneous turning and boring roughing pass of a CNC Lathe. Response Surface Methodology (RSM) is defined as a collection of statistical

and mathematical techniques useful for developing, improving and optimizing processes [1]. The deliverables that are expected to be achieved from by this research and the application of RSM are:

- Implementation and data acquisition from numerous sensors.
- Develop multiple linear regression models for captured sensor statistics.
- Find optimal settings for production at the Red Lion facility.

In Chapter 2, a comprehensive overview of the methodology used in this study will be described. Section 2.1 will begin with an overview of the fundamentals of turning and boring theory. It is of importance to first understand the process that is to be optimized because the factors that are to be used for the optimization need to be determined either by experimentation or from previous literature. Following the theory review, a summary will be given of current research that is being performed that utilizes multiple sensors and RSM to find optimal machining parameter settings for the given operation. Although much research is being conducted, none covers the simultaneous turning and boring cutting operation, or uses the wide variety of sensors implemented in this research. Another area that is also covered in the scope of the optimization is that of tool wear (section 2.2) and tool life (section 2.3). An overview will be given of current trends that are being used for measuring and predicting tool life and tool wear. In section 2.4 the cost of producing a part will be discussed in detail using a function commonly referred to as the cost function. The cost function helps determine a balance between tool life and cutting time that yields a minimum cost.

In section 2.5 a detailed explanation will be given explaining the theory behind RSM. This will include the mathematical modeling of how the multiple linear regression models are created, plots that are used in demonstrating both the model and its adequacy, and techniques that are used to find optimal machine parameter settings. Also an explanation will be given of why RSM is to be applied over a different optimization technique. After the RSM theory is explained the designs used in this research will be explained. Since RSM is a broad topic encompassing various designs that may be used, it is important to discuss what designs were chosen and how they were applied. The last section of Chapter 2 (section 2.6) will give a summary of an important function that was applied in the optimization of the machining process. This function is known as the desirability function which is commonly used in optimization of manufacturing processes.

Chapter 3 will focus solely on sensor setup and data acquisition. Section 3.1 will focus on the sensor selection for this research and on the reasons why these sensors could help determine optimal machining parameters. A broad range of sensors are used in this study to limit the amount of noise that could be presented by nuisance factors. In section 3.2 a description will be given of the data acquisition system (DAQ) that was used for the numerous sensor signals that were captured. To capture all of these sensor signals simultaneously a LabView program was created to set the different sampling frequencies required and store the data in the DAQ's hard drive. Another program was also created in LabView in order to locate and capture the statistics needed for the optimization.

The important results obtained by using RSM are discussed in Chapter 4. Section 4.1 focuses on the empirical models gathered from the designed experiments. Only models which are key to the optimization are covered. Section 4.2 discusses the optimal settings found by using the empirical models found in section 4.1.

The results obtained from the empirical model and optimization can be applied to an adaptive controller. The future research to be performed will be described in detail in Chapter 5.

2 CHAPTER 2 – METHODOLOGY

2.1 Literature Review

Advances in manufacturing technology today have led to improved production in facilities, while still using the same fundamental processes such as turning and boring. Since the nature of the machining is the same, economic implementation of new technologies to primitive machines is feasible. There is a demand in the industry to reduce production costs that has driven many major manufacturers to automate operations previously performed by skilled operators [2]. By improving a machine's sensing technology, many of the tasks usually performed by an operator, such as monitoring the tool condition, metalworking fluid levels, and surface quality may be automated. Before the process is automated, it is important to find machine parameter settings that will yield optimal conditions that will produce parts fast, extend the life of the tool, and take into account the labor fees of the factory.

Most metal parts used today are produced by a traditional machining operation such as turning, boring, milling, surface grinding, etc. All over the world over $100 billion dollars are spent annually on metal removal processes and 10% of the material produced by machining goes to waste [3]. The operating conditions for a machining operation are can be determined by a manufacturing handbook or specified by the tool manufacturer. These conditions are not optimal as metals are produced by several different methods with great differences in hardness and dimensions causing more scrap parts. To overcome these drawbacks, much research has been conducted to establish a description of the machining parameters by mathematical modeling [4]. Mathematical modeling of the behavior of a measured response against the selected machining

parameters is possible through techniques such as Design of Experiments. Before entering into a discussion of how mathematical models are implemented in manufacturing, a brief overview will be given of the turning and boring operations.

Both turning and boring are single-point machining processes which are normally used to machine castings and forgings that require precise dimensional tolerance and a uniform surface finish [5]. The tools normally used for turning and boring are either triangular, diamond, or square shaped carbide inserts and they are clamped down onto a tool holder. A part called a shim normally separates the tool holder from the actual cutting tool. The carbide insert used in this research for the OD turning included a total of four cutting edges, while the ID boring tool included a total of eight cutting edges, due to its square shape. Two axes of machining are introduced in the turning operation and an additional two are introduced in the boring operation making the simultaneous turning and boring operation a four axis machining process. The axes that run perpendicular to the spindle are commonly labeled as the X axes. The axes that run parallel to the work piece are commonly labeled as the Z axes.

The cutting operations performed by a CNC Lathe are normally described by the machining parameters such as the spindle speed, feed rate and depth of cut. There are also several other ways to express the cutting operation such as using the cutting speed instead of the spindle speed but by doing some simple arithmetic the same terms can be derived. The spindle speed describes the rotational speed of the spindle. For this research the feed rate can be expressed as the rate in which the tool moves parallel to the work piece in the Z axes. For this operation, the feed rate is a function of the spindle speed. For example, if the feed rate is 0.02

in/rev the tool will traverse 0.02 inches in the time the spindle performed one complete revolution. The depth of cut is the only factor in this process that may be different for either the turning or boring operation. The depth of cut for the turning operation can be calculated simply by subtracting the outer diameter of work piece from the desired diameter and then dividing by two to obtain the depth of cut. The same is done for the boring operation except that in the boring operation one subtracts the desired diameter from the inner diameter and divides by two.

By using the described machining parameters that control the cutting operations the Response Surface Method can be applied in order to model responses and optimize the process. Even though Response Surface analysis will provide an empirical model for the cutting operation, the fundamental cutting mechanics will explain if the derived empirical model has meaning. To explain the dynamics of the metal removal process, Tlusty [6] divides the cutting forces into three components, the feed force, the radial force, and the tangential force. The feed force is the force purely in the direction of the Z axes of the lathe. The radial force is the force acting on the X axes of the lathe. The tangential force is the largest force because it the force is exerted from the spindle rotation onto the tool. Tlusty mentions that for most practical purposes the cutting force is determined through empirical formulas derived from cutting tests [6] much like what is being conducted in this research. The cutting forces can be defined as a function of the chip width (b) and the chip thickness (h) and a material constant (K_s). The most general form of the tangential force can be seen in Equation 1.1.

$$F_T = K_s bh = K_s af_r \tag{1.1}$$

In Equation 1, the tangential force is mentioned as a function of the chip width and chip thickness and also as a function of the parameter settings. The chip width corresponds to the feed rate (f_r) and the chip thickness corresponds to the depth of cut (a). As mentioned, the general force calculations are generic and should give the engineer a region of where the forces should act. It is important to carry out experiments to determine the more accurate forces. Some similar experiments will be explained later on, in this section.

During the simultaneous metal removal operation one of the major causes of scrap work pieces is the induction of chatter. Chatter is considered a phenomenon caused by unstable vibrations when using a set of cutting conditions. When chatter occurs, unstable chaotic motions of either the tool or the work piece are seen causing unusual force fluctuations. Chatter may cause tool wear, tool breakage, and poor surface finish thus diminishing the dimensional accuracy of the work piece [7]. Much research is being conducted towards diminishing chatter vibrations. During the simultaneous cutting process, chatter was induced during the boring operation several times. The cause of chatter was the eccentricity of the work piece. The minimum cutting diameter for the inner diameter had to be 0.100 in for chatter not to occur. Conservative cutting conditions are normally used on the shop floor which result in lower material removal rates and loss of productivity [5]. In this research part of observations in the experimental space will determine if chatter is induced using a specific set of cutting conditions.

Several attempts have been made to monitor metal removal operations. Bouacha et al [8], applied Response Surface Methodology to investigate the effects of cutting parameters such as cutting speed, feed rate and depth of cut on cutting forces and surface roughness in hard turning.

Hard turning is considered the material removal process of a work piece of a hardness which is higher than 45 HRC. By using a Taguchi orthogonal array, Bouacha et al were able to define equations for the surface roughness and the cutting forces for their operation. They noticed that as the feed rate and depth of cut are increased, the forces are higher. They also established a strong correlation between the feed rate and the surface roughness. This is expected as a higher feed rate generally leads to a poor surface finish. One of the major differences between the research performed and Bouacha's research is that in this research multiple sensors are used to monitor the cutting operation. Much research is being conducted to monitor the cutting operation via multiple sensors.

Kuljanic et al [9], attempted to use a rotating dynamometer, accelerometers, acoustic emission, and power sensors to monitor the onset of chatter in milling operations. By using more sensors he was able to obtain more accurate results for chatter identification as opposed to using a single sensor signal. For the purpose of his studies the force and acceleration measurements proved to be best at chatter detection, while the acoustic emission sensor and power sensor did not provide much change when chatter was induced. By using this multi-sensor approach, very high levels of accuracy for chatter detection were obtained thus producing a more robust system.

Another project towards the improvement of machine monitoring was performed by Kwak et al [10] who analyzed the power and surface roughness of cylindrical grinding of steel using the response surface method. By applying the response surface method, mathematical models were derived for both the power and surface roughness.

Other than the few mentioned, several research projects have proved useful in either machine monitoring or using response surface methodology to improve the machining process [11-17]. There are several areas in which this research is novel which include:

- Number of sensors used combined with data capture of all sensor signals.
- Analysis of the simultaneous turning and boring operation.
- Response surface analysis of AISI 4137 forged steel for simultaneous cutting operation.

2.2 Tool Wear

In an orthogonal cutting operation several mechanisms can cause failure of the tool. These mechanisms can include abrasive/flank wear, built-up edge, thermal/mechanical cracking, cratering, thermal deformation, chipping, notching, and fracture [18]. The most common measured type of wear in orthogonal cutting is the flank wear. In this research the flank wear is measured through a microscope. The norm for the limit of flank wear allowed for a tool is set to 0.2 mm for finishing operations and 0.5 mm for roughing operations [19]. Since the operation that is being observed is roughing the allowable tool wear region is set to 0.5 mm. This becomes important when fitting a tool life function. Several attempts have been made to measure the flank wear of the cutting tool during online machining. Choudhury was successfully able to predict the flank wear of the tool by using the ratio between the feed force and the tangential force [20]. Kopac was able to achieve tool wear monitoring through a microphone [19]. Several papers have also been published on the use of acoustic emission sensors for the monitoring of tool wear [21-23].

Although the focus of the current research is not to measure tool wear during the simultaneous cutting operation, it is possible that the models derived for tool wear can be correlated to other models such as force, temperature, sound etc. Tool wear prediction plays a vital role in the optimization of the cutting process because even for modern machine tools 20% of the downtime can be attributed to tool failure [24], thus reducing the productivity of a facility leading to profit losses.

2.3 Tool Life

Tool life is one of the most researched topics in metal removal operations as it is inversely proportional to the cost of creating a finished product. The most common equation used to calculate tool life is referred to as the Taylor Tool Life equation shown in Equation 2.1.

$$T = \frac{C}{v^p f^q} \tag{2.1}$$

The tool life (T) is expressed a function of the cutting speed (v) and the feed rate (f). The rest of the terms (C,p,q) are constants that are calculated experimentally. For the purpose of this project the tool life equation was calculated using a factorial design. Similar tool life estimation was performed by Amaitik et al [25]. The method behind this calculation is performed by linearizing the Taylor Tool Life equation as shown below in Equation 2.2.

$$\ln T = \ln C - p \ln v - q \ln f \tag{2.2}$$

Since the linearized Taylor Tool Life equation is a linear equation, it does not require a second order model to represent the function. In terms of a design of experiments approach, the response of the Taylor Tool Life can be described as Equation 2.3.

$$y = \beta_0 + \beta_1 x_1 + \beta_2 x_2 \tag{2.3}$$

From the equation above it can be seen that all of the coefficients from the Taylor Tool Life can be calculated using a factorial design consisting of a minimum of four tool life experiments. A design of experiments was created to calculate the tool life of the OD tool because the OD tool life is much shorter than the ID tool life due to its higher material removal rate. To ensure that a precise tool life equation was estimated, a two level factorial design was created. The design of experiments to measure tool life lied within the same range as the Response Surface analysis that is performed in this research. The two level factorial design was repeated twice to ensure reliable measurements. The tool life could be estimated with an R-sq. value of 98.34% using the factorial design. To convert the Taylor tool life equation from logarithmic units to exponential units as seen in Equation 2.1 a conversion had to be done from logarithmic units to exponential units. The final tool life equation for the OD tool can be seen in Equation 2.4.

$$T(OD) = \frac{1.09933 \times 10^{10}}{v^{4.625846} f^{3.816334}} \tag{2.4}$$

The Taylor Tool Life equation derived for the OD tool becomes important for the cost model that is derived in the Response Surface experiments. It was used in the analysis of

simultaneous cutting operation by adding the results obtained from this equation into the Response Surface results. From there, an estimate of the tool life can be made using the factors used in this experiment. Because of the limited experimental region observed, a quadratic model is enough to estimate tool life when applied to the Response Surface experiments performed. The results from the tool life model are reflected in the cost estimation.

2.4 Cost

One of the key goals of this project is to reduce the cost of machining. It is easy to think that one could have optimal settings by increasing the production speed by increasing the spindle speed and feed rate, but if the tool repeatedly fails rapidly then there will be little to no cost savings. To understand a general perspective of cost estimating for manufacturing, Malstrom [26] defines that the general manufacturing costs of a facility should be a function of the direct labor, direct material costs, factory expenses and general expenses. While labor and material costs are straight forward factory expenses could be explained as cost of rent, air conditioning/heat, utilities, machines etc. The general expenses can be defined as the cost of design engineering, purchasing, and other back office related costs.

To narrow down on just the cost of a part (C_p), Tlusty [6] defines the cost of a part as a function of fixed costs (C_{fix}), machining costs (C_m), and the tooling costs (C_t). The equation derived by Tlusty is shown below in Equation 2.5.

$$C_p = C_{fix} + C_m + C_t \tag{2.5}$$

In this equation the two controllable parts are the cost of machining and the tooling costs. The costs of machining are associated with the labor fees of the shop and the time it takes to produce a part. The tooling costs are associated with price of the cutting insert and the time required to change the tool. Srinivas et al [4], take this function one step further by adding idling costs which include the time that the operator takes to change the work piece. The equation used to determine the cost of each experiment is shown in Equation 2.6.

$$C_p = t_i r_m + t_m r_m + \frac{(t_{ch} r_m + C_{te}) t_m}{T(OD)} \tag{2.6}$$

In this equation t_i represents the idling time in minutes, t_m represents the machining time in minutes, t_{ch} represents the tool changing time in minutes, r_m represents the rate of machining in US dollars, C_{te} represents the cost of the tool edge in US dollars, and $T(OD)$ represents the OD tool life in minutes. All of the terms in the cost equation were estimated using the costs associated with the Red Lion facility. The cost equation used for this research is shown in Equation 2.7. The Cut Time is derived from the empirical model shown in section 4.1.1.

$$C_p(\$) = 1.38 \times \frac{(CutTime)}{60} + 0.5 \times 1.38 + \frac{(3.38 \times \frac{CutTime}{60})}{\frac{1.09933 \times 10^{10}}{v^{4.625846} f^{3.816334}}} \tag{2.7}$$

The cost function shown in Equation 2.7 should suffice for the purposes of this research. Expansion of the cost function is possible with the incorporation of the boring bar carbide insert. Although not applied in this research the equation derived for simultaneous turning and boring is

shown in Equation 2.8. The only difference between the cost functions is that the cost of tool, the tool changing time, and the tool life, correspond to either the OD turning operations or ID boring operations.

$$C_p = t_i r_m + t_m r_m + \frac{(t_{chOD} r_m + C_{teOD}) t_m}{T(OD)} + \frac{(t_{chID} r_m + C_{teID}) t_m}{T(ID)} \tag{2.8}$$

The cost function is always an estimate of what is the cost to create a part. To increase the accuracy, the amount of scrap parts, the electricity costs of the facility, rapid tool failures and many other factors can be considered.

2.4 Response Surface Method

Due to the complex system dynamics of simultaneous turning and boring, an analytical approach to finding optimal machine parameter settings would be lengthy and will not take into account the variability of the system. The Response Surface Method has been proven useful numerous times in the manufacturing field. In this section an in depth explanation will be given of the theory behind RSM and the approaches used to find optimal results. The usual approach to using RSM involves a three step process. First a set of experiments is designed that will yield adequate and reliable measurements of the responses of interest. After the experiments are conducted mathematical models that best fit the data are chosen followed by determining optimal settings of the experimental factors that produce the maximum or minimum value of the response [27].

Although the process seems to be straightforward it is important to note that it is not just performed once, it is rather an iterative method performed with several different types of designs

that ensure that the approximate response of the system is true within the region of interest. In the first round performed it is important to determine which of the factors are crucial to the machining process. Normally, less experiments are performed with more factors thus resulting in a loss of accuracy, yet the main factors that affect the system will be determined thus eliminating those factors which are not important. This is commonly known as the “screening stage”.

After all factors that impact the desired responses are determined and a region of experimentation near the location of optimality is found, a more sophisticated set of experiments is used to build the mathematical models of the system. This set of experiments will require more experimentation yet will output highly accurate models. From these models the local optimums within the region of experimentation can be found and the tradeoffs of each response can be identified.

After finding the optimal settings, if the experimenter has enough capital, a repeat of the second set of experiments can be run in order to validate the results. Now that the experimental process has been established, the theory behind how RSM functions will be explained.

Multiple linear regressions are used in RSM to build empirical models that approximate the true response of the system. To be able to build the regressions it is important to first define what are considered the factors that are to be controlled and what responses will be monitored. In CNC operations the user is allowed to control the speed of the spindle rotation, the feed rate of the tool progression through the work piece and the depth of cut. Since the turning and boring passes are performed simultaneous then the factors of spindle speed and feed rate are the same but the depths of cut may vary thus resulting in a total of four factors which are termed the

spindle speed (x_1), feed rate (x_2), OD depth of cut (x_3), and ID depth of cut(x_4). The different designs of experiments used will vary these four factors in order to build the mathematical models for the responses (i.e. force, temperature, vibration, etc.) only based off of these controllable factors. An example of this is shown in Equation 2.9.

$$y = f(x_1, x_2, x_3, x_4) + \varepsilon \tag{2.9}$$

The ε term in the equation above is also known as the statistical error which represents the sources of variability in the system that are not accounted for in f [1]. To expand on the equation above, the final model that is to be created based off the designed experiments is second order in nature due to the attempt of finding the stationary point in the function whether it be a maximum, minimum, or saddle point. The final model should have first and second order terms along with their regression coefficients. An example of a generalized equation for a second order model is shown in Equation 2.10.

$$y = \beta_0 + \sum_{i=1}^{k} \beta_i x_i + \sum_{i=1}^{k} \beta_{ii} x_i^2 + \sum \sum_{i<j=2}^{k} \beta_{ij} x_i x_j + \varepsilon_i \tag{2.10}$$

In order to estimate each of the regression coefficients (β), the method of least squares is used. The least squares method in this application chooses the regression coefficients so that the sum of the squares of the statistical error is minimized [1]. Since the least squares method is applied for various experimental conditions it is better to define the least squares application in matrix notation as seen in Equation 2.11. In Equation 2.11, y is a vector that represents the

response at different levels, X is the design matrix which represents all of the factor levels in the experimental design, β is the regression coefficient vector and ε is the statistical error vector.

$$\mathbf{y} = \mathbf{X}\beta + \varepsilon \tag{2.11}$$

The least squares function applied to minimize the statistical error is shown in Equation 2.12.

$$\mathbf{L} = \varepsilon^{\mathbf{T}}\varepsilon = (y - X\beta)^T (y - X\beta) \tag{2.12}$$

Equation 4 must then be expanded. This is shown in Equation 2.13.

$$L = y^T y - 2\beta^T X^T y + \beta^T X^T X\beta \tag{2.13}$$

To minimize the error, the differential of Equation 5 with respect to the regression coefficients (β), must be performed and set equal to zero. This equation is then solved for the least square estimator. The least square estimator vector (b) is shown in Equation 2.14.

$$b = (X^T X)^{-1} X^T y \tag{2.14}$$

The least squares estimator is useful in determining the regression coefficients but will not identify if the values gathered are statistically significant. In order to test for statistical significance analysis of variance (ANOVA) must be performed. The process of performing ANOVA is based on hypothesis testing to determine the linear relationship between the response (y) and the factors (x_i). Hypothesis testing is shown below in Equation 2.15.

$$H_0 = \beta_1 = \beta_2 = \ldots = \beta_k = 0 \text{ (Null Hypothesis)} \tag{2.15}$$

$$H_1 = \beta_j \neq 0 \text{ (Test Hypothesis)}$$

Rejection of the null hypothesis would prove that one of factors contributes significantly to the approximate model created. In order to test this hypothesis the Fisher F test is performed. The F test in multiple linear regressions is performed by partitioning the total sum of squares into the sum of the squares of the regression and the sum of the squares of the residual error. The F test is shown in Equation 2.16.

$$F_o = \frac{SS_R / k}{SS_E / (n-k-1)} \tag{2.16}$$

In Equation 2.16, the sum of the squares of the residual (SS_R) is divided by the degrees of freedom dedicated to the regression (k). The sum of the squares of the error (SS_E) is divided by the degrees of freedom of the residual (n-k-1). The variable n represents the total degrees of freedom but one degree of freedom is always dedicated to the intercept, thus the total possible available degrees of freedom is always n-1.

Now that the F value is calculated, the P-value can be used to decide whether or not to reject the null hypothesis. The null hypothesis will be rejected if the P-value for the F statistic is less than the significance level (α). The significance level is extremely important in deciding whether or not the given factors will be important. In the screening stage a value of α = 0.1 is used to determine whether or not the chosen factor is significant. In the more complex set of

experiments, where more tests are performed to obtain a more accurate model, $\alpha = 0.05$ is chosen to determine if the factor is really significant.

The most significant component of the RSM is choosing the correct design of experiments to follow, in order to build the mathematical models and optimize accordingly. In this research, a 2^4 factorial design is used for screening followed by three face centered central composite designs that are used to build and check the models created.

The 2^4 design was used to screen the initial system parameter settings to decide if the upper and lower levels of the factors were feasible. The initial parameter settings were based around the Red Lion facility settings. These screening experiments are extremely useful to determine what are the main effects and interactions of each one of the responses. Also centerpoint runs were added to check for curvature. The center point runs consist of running all of the four system factors at their center level, which in coded terms results to x=0. Before each experiment of the factorial design was performed, initial cuts were performed on the work piece both in the inner and outer diameters to remove the rust layer and leave the work piece at defined known diameters.

Three face centered central composite designs were used to build the mathematical models and optimize the machining process. The central composite design consists of $2^k + 2k + n_c$ runs. The central composite designs are the most popular type of design of experiments due to their effectiveness and minimal number of runs to build second order models. This design of experiments is an expansion about the factorial design seen in the screening experiments but

axial points are added to better determine the second order model. The reasoning behind using the face centered cube relies on the stringent operating conditions.

Each one of the three face centered central composite designs was defined as Response Surface I (RSI) , Response Surface II (RSII), and Response Surface III (RSIII). RSI followed the same trend as the screening experiments by including the initial cuts on the work pieces. RSII and RSIII perfectly imitated the cutting conditions at the Red Lion facility thus did not include the initial cuts. The main reason for performing RSIII was to verify that the models from RSII were accurate.

2.5 Desirability Function

One of the most useful approaches when performing optimization of multiple responses is to use the desirability function approach [1]. The methodology behind the desirability approach is to convert each one of the responses (y_i) into an individual desirability function (d_i). The range for the desirability function is shown in Equation 2.17.

$$0 \le d_i \le 1 \tag{2.17}$$

If the response is at its chosen target then the desirability function will equal 1. If the response is outside of the desirability region then the desirability will equal 0. To maximize the overall desirability, Equation 2.18 is implemented. The term *m* in Equation 2.18 represents the responses.

$$D = (d_1 d_2 d_3 .. d_m)^{1/m} \tag{2.18}$$

Usage of the desirability function requires careful selection of the region one is trying to target. This is why it is important to use overlaid contour plots to determine what area is near optimal operating regions. Three different operation constraints can be chosen while using the desirability function approach. One can choose to minimize, maximize, or attempt to acquire a target number for the response. Most of the applications for this research require minimization of the response. The individual desirability function for a response for minimization is shown in Equation 2.19.

$$d = \begin{cases} 0 & for \quad y < L \\ \left(\frac{y-L}{T-L}\right)^r & for \quad L \le y \le T \\ 1 & for \quad y \ge T \end{cases} \tag{2.19}$$

In the equation above, L represents the lower bounds, T represents the target value and r represents the weight applied. Depending on the importance of the desirability of each measure, a weight can be placed to put more emphasis on that term being closer to the target value. Embedded into Minitab 16 software is a Response Optimizer package where the user can input the lower bounds, upper bounds, target values, and weights. The Response Optimizer will then calculate the maximum desirability.

3 CHAPTER 3 – EXPERIMENTAL SETUP

3.1 Sensor Setup & Installation

Phase I of the simultaneous turning and boring optimization research, focused solely on sensor and data acquisition setup. The sensor setup process began by narrowing down which sensors were to be used for the monitoring of the operation. The future of this research (Phase III) will correlate cost effective sensors such as a power meter, microphone and thermocouples to more complex sensors like piezoelectric accelerometers, force sensors, and acoustic emission sensors. By performing this correlation, a cost effective adaptive control system for each machine becomes feasible for a large manufacturing facility.

Not all of the sensors installed on the lathe were modeled using Response Surface Methodology as they did not play a role in the optimization of the machining operation. The multitude of sensors added combined with the ability to capture the data simultaneously is one of the major breakthroughs of this research. For this reason, all of the sensors installed on the CNC lathe will be described.

The sensors used to monitor the simultaneous roughing operation can be classified into two different styles of sensors labeled either combined or turret specific. Combined sensors measure the machining operation without specifically either addressing the upper and lower turrets, while individual sensors measure a parameter specific to either the lower turret assembly or the upper turret assembly. The sensors that fall into the combined sensors category are the power meter, microphone, metalworking fluid flow meter, metalworking fluid thermocouple and

video camera. A basic diagram of the combined sensor setup is shown in Figure 3-1. It must be noted that this diagram does not expand upon the data acquisition setup which is in section 3.2.

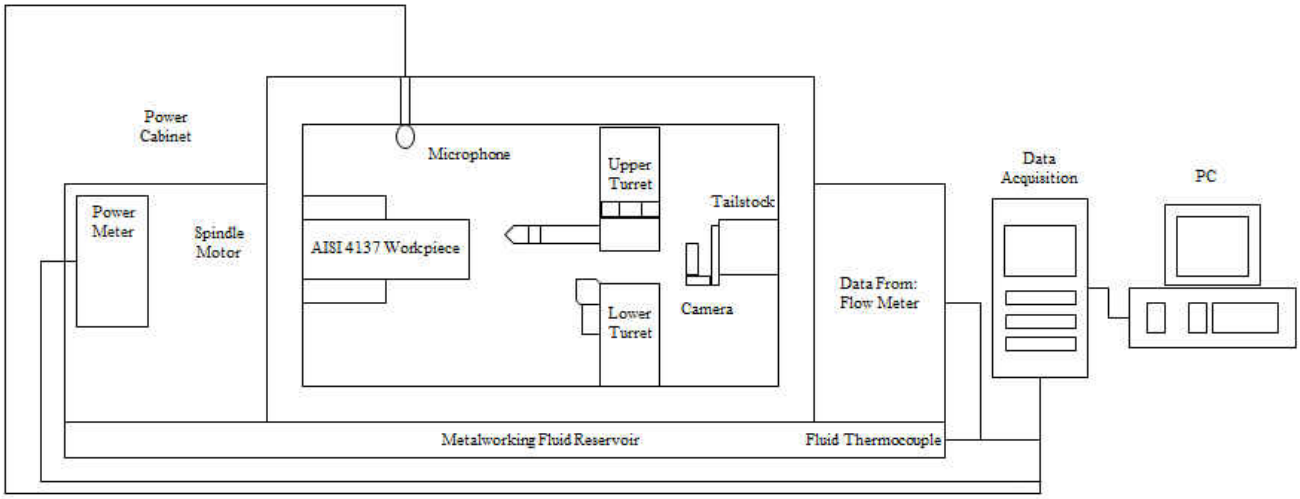

Figure 3-1: Diagram of Combined Sensor Setup

The turret specific sensors pertain to measurements of either the ID boring assembly or OD turning assembly. The turret specific sensors for the OD turning assembly consist of a tri-axial dynamometer, a tri-axial accelerometer, an acoustic emission sensor, and a tool thermocouple. The turret specific sensors for the ID boring assembly consist of tri-axial force sensors, a tri-axial accelerometer, an acoustic emission sensor and a tool thermocouple. A basic diagram for the ID boring assembly can be seen in Figure 3-2. In Figure 3-2, it must be noted that the sensors pre amplifiers, signal conditioners, and specific data acquisition connectors are not shown.

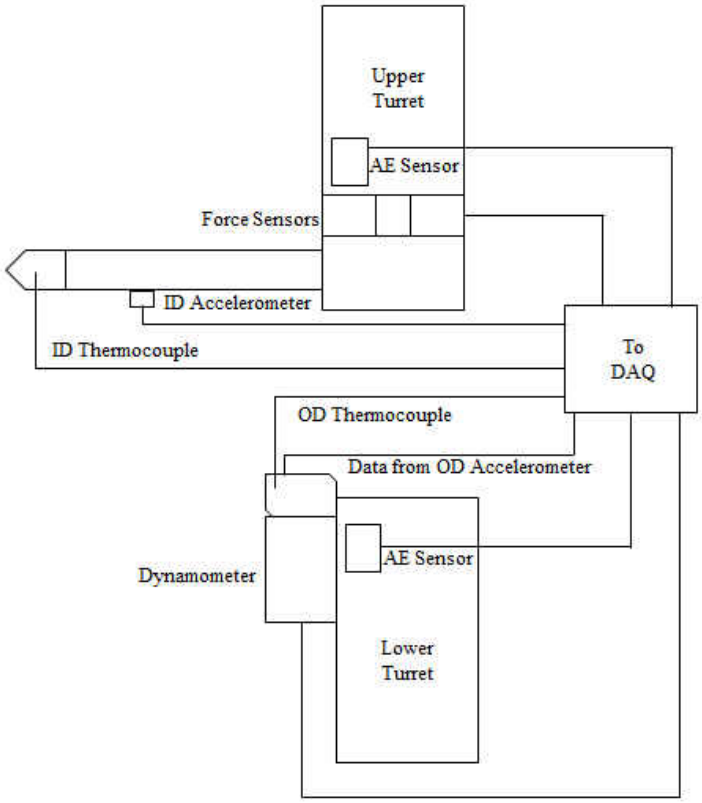

Figure 3-2: Diagram of Turret Specific Sensor Setup

In the next subsections, all of the sensors used to monitor the machining operations will be described in further detail. The next section of the experimental setup will explain the data acquisition setup and program used for data acquisition. The final section of this chapter will be focused on the experimental design used to model and optimize the machining operation.

3.1.1 Metalworking Fluid Flow Meter

The CNC lathe is equipped with an internal metalworking fluid system, which pumps the fluid into the upper and lower turret assemblies. Being able to monitor the fluid flow, will determine if there are significant fluctuations in the volumetric flow rate during each experiment

or that the flow rate can be treated as a constant value. If large fluctuations are seen, the sensor signals can then be correlated with the output temperature of the thermocouples and the tool wear.

A rotating paddle wheel volume flow meter manufactured by Signet was used to monitor the flow of the metalworking fluid through both the upper and lower turrets. The flow meter was installed in the piping assembly powered by the pump sump in the metalworking fluid reservoir. A gate valve was also installed to control the flow rate if necessary. The sensor output was an analog current signal ranging from 4 – 20 mA and was connected to the data acquisition through a National Instruments current input conditioning module in the signal conditioning carrier. The data received from the flow meter was sampled at 10 Hz, as changes in metalworking fluid are generally slow. The installed sensor can be seen in Figure 3-3.

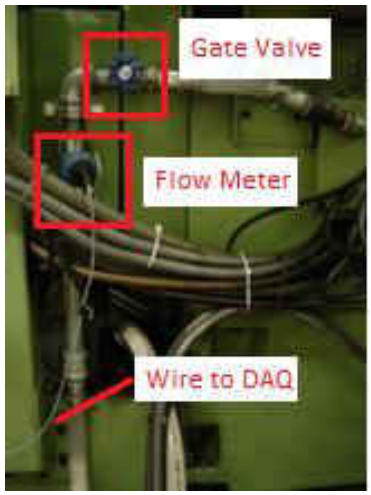

Figure 3-3: Flow meter installation

3.1.2 Thermocouples

To measure the temperature of the OD & ID tools, Omega Engineering K-type thermocouples were installed in the shim of the OD and ID tool holders. To allow for installation of the thermocouples, the tool shims were machined via electric discharge machining to allow for a groove of a length of 1.5 mm and a depth and width of 0.5mm. The grooves for the ID and OD thermocouples can be seen on Figure 3-4. Thermal conductive grease was applied to the groove before the thermocouple was placed in position.

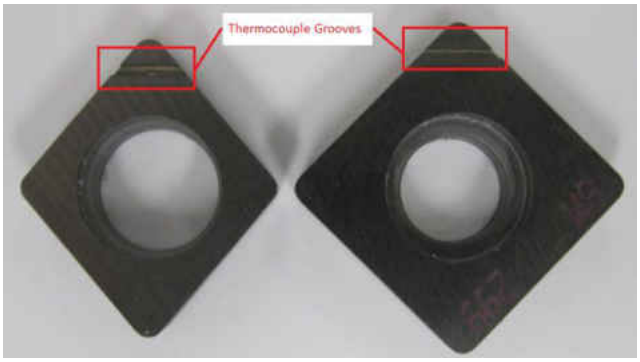

Figure 3-4: (Left) Machined OD tool shim (Right) Machined ID tool shim

The location for the thermocouple positioning was chosen to minimize the risk of exposure to metal chips and metal working fluid flow. Several problems were observed from the chosen positioning of the thermocouples. The constant tool replacement from experiment to experiment slightly shifted the position of the thermocouples. Also, even though the thermocouple tip did not suffer any damage during cutting, the wires were continuously slashed by metal chip debris.

Another thermocouple of the same type was installed in the metalworking fluid reservoir to monitor any rises in temperature during experimentation. The thermocouples were routed through the internal components of the lathe and were connected to a National Instruments thermocouple module in the signal conditioner carrier. The sampling rate of all of the thermocouples was 10 Hz.

3.1.3 Boring Bar (ID) Force Sensors

To monitor the tri-axial cutting forces on the boring bar during machining, a set of 9066A4 Kistler group piezoelectric force sensors were installed on the upper turret assembly. The set of four force sensors could not be installed directly on the upper turret assembly, and required an adapter assembly for installation. Force sensor adapter plates were manufactured using AISI 1018 steel plates with the thickness and surface finish requirements specified by Kistler. To allow for metal working fluid passage through the force sensor adapter assembly, a connection using barb hoses and vinyl tubing was made to the steel plates. The force sensor adapter assembly was then positioned directly on the upper turret with the boring bar tool holder sitting above the force sensor assembly. The assembly was held together by four M16 bolts of 120 mm in length torqued to the Kistler specified preload conditions. The force sensor assembly and turret mounting are shown in Figure 3-5.

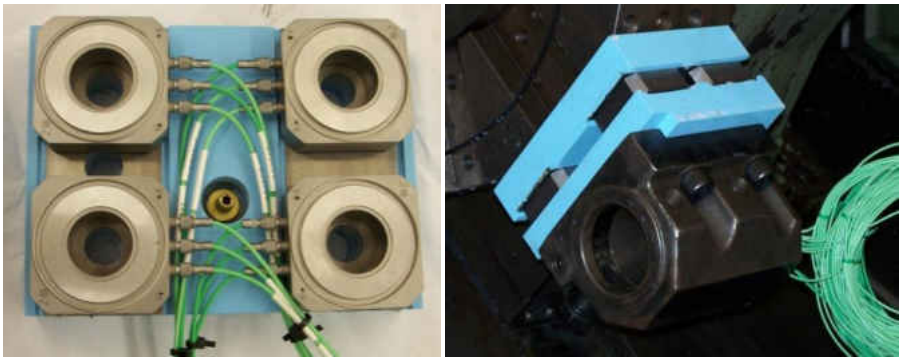

Figure 3-5: (Left) Force sensors and hose for fluid passage (Right) Mounted assembly

To ensure that the modified boring bar assembly would possess the same system dynamics as the Red Lion facility, impact hammer testing was performed on the boring bar. The results from the impact hammer tests resulted in frequencies very close to the Red Lion setup. The boring bar held an overhang of 10” on average. To match the natural frequencies, the boring bar was shifted to having an overhang of 9.875”.

Each one of the wires shown in Figure 3-5, represent the Fx, Fy, Fz axis measurement of each force sensor. Each one of the wires was routed to one of the three summing blocks for the three axes measured (Fx, Fy, Fz). The summing blocks were connected to a Kistler 5814B charge amplifier. The charge amplifier contains a 4.7 kHz low pass filter and allows for control of the measurement range. The sampling rate for the force sensors was 20 kHz and the data output of the force sensors (routed through the charge amplified) was provided through BNC cables, thus a National Instruments BNC connector block was used to capture the data.

3.1.4 OD Dynamometer

To measure the tri-axial forces on the outer diameter cutting tool a Kistler 9121 tool holder dynamometer was used. The dynamometer measures the three orthogonal components of the X,Y,Z forces acting on the cutting tool via piezoelectric elements. This specific dynamometer was designed to be used on turret lathes much like the lathe used in this research but it would not fit into the lathe without an adapter. An adapter was manufactured out of AISI 1018 steel to fit the dynamometer onto the lathe. Figure 3-6 shoes the dynamometer, adapter plate, bolts, and tool holder ready to be mounted onto the lathe.

Figure 3-6: (Left) Dynamometer assembly (Right) Dynamometer mounted on lathe

The OD dynamometer was connected to the Kistler charge amplifier of the same style as the ID force sensors and then routed to a National Instruments BNC connector block. The sampling rate for the OD dynamometer was 20 kHz.

Similar to the boring bar assembly, frequency analysis was also performed on the OD turning assembly to determine if the system dynamics have shifted. The OD turning assembly is much stiffer than the ID turning assembly. Because of the rigidity of the system, the natural

frequencies of OD turning assembly could not be accurately excited. The frequency limit of the impact hammer used to excite the natural frequencies is 5 kHz. From the results, it can be deduced that any instability caused by the modification would be caused by the boring bar assembly modification over the OD turning assembly.

3.1.5 OD & ID Accelerometers

To measure the vibrations during machining, two PCB Piezotronics 356B21 tri-axial accelerometers were mounted on the lathe. The location for the accelerometer mounting is critical as placing the sensor far from the cutting operation will cause faulty readings as dampening will have occurred. The simultaneous roughing operation of forged work pieces causes a heavy amount of vibration, so accelerometers of a sensitivity of 10 mV/g were chosen to keep the accelerometers within their operating range.

The accelerometers for both the turning tool and the boring bar were installed as close as possible to the cutting tool insert. To mount the accelerometer on the turning tool, a hole was drilled and tapped in the rear side of the OD tool holder. The distance from the tool holder to the tool tip was 3 cm. The accelerometer was mounted in the hole by a threaded stud provided by PCB Piezotronics. Wax was used to cover the cable connections, although the cables were hermetically sealed. The accelerometer placed on the OD tool holder can be seen in Figure 3-7. The location of the accelerometer is adequate because it ensure that few chips and little metalworking fluid will contact.

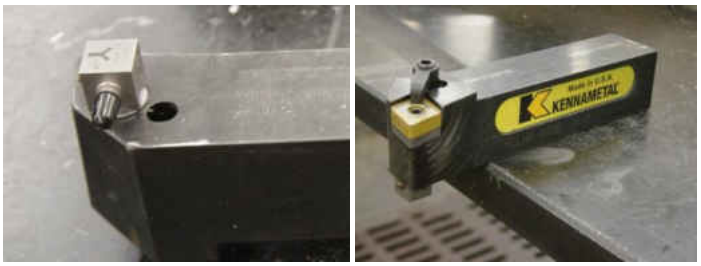

Figure 3-7: (Left) Rear side of OD tool Holder (Right) Complete OD tool holder assembly

The geometric structure of the boring bar did not allow for a similar installation of the ID accelerometer. The boring operation is also an internal operation, so being clear of any machining debris is not a possibility. The accelerometer for the boring bar requires a small circular section to allow for an accelerometer to be screwed onto the boring. Also, a groove was made along the boring bar to allow for cable routing to the data acquisition system. To further protect the accelerometer, the boring bar was wrapped with duct tape, to prevent any debris or coolant to enter. The boring bar accelerometer assembly can be seen in Figure 3-8.

Figure 3-8: Boring Bar Accelerometer Assembly

The two accelerometers were connected to a PCB signal conditioner that provided the accelerometers with current excitation. The signal from each axis was then recorded via BNC connectors connected to a National Instruments BNC connector block.

3.1.6 OD and ID Acoustic Emission Sensors

Due to the growing popularity of monitoring acoustic emissions in the metal removal field, a Physical Acoustics R3a acoustic emission sensor was mounted on the upper and lower turrets. The AE sensor data will be powerful for performing correlation analysis with tool wear and tool breakage. The AE sensors were installed on the upper and lower turrets via a magnetic hold down provided by Physical Acoustics. The OD AE sensor can be seen in Figure 3-9.

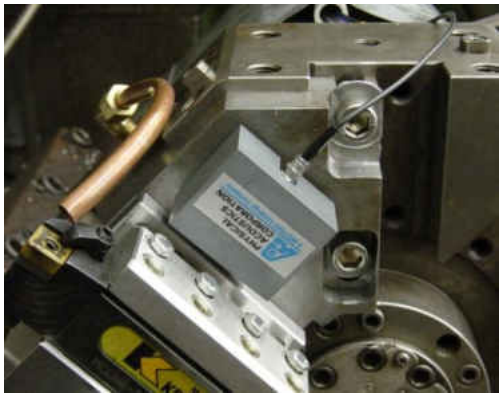

Figure 3-9: OD AE Sensor Setup

Both time and frequency domain analysis of the AE sensors is of interest. The frequency range of interest for the AE sensors was between 100 – 400 kHz so a bandpass filter was used to minimize frequencies outside that range. A power supply was used to power a signal pre-amplifier purchased from Physical Acoustics. The sampling rate chosen for the AE sensors was 800 kHz which satisfies the Nyquist criteria. The response from the AE sensors was routed via BNC cables to a National Instruments shielded connector block. Each one of the sensors was provided its own data acquisition card.

3.1.7 Power Meter

To measure the total three phase electrical power consumed by the lathe during machining a Load Control PH-3A Hall Effect power meter was installed in the electrical breaker cabinet of the lathe. The measurements from the power meter will allow for statistical measurements such as the average power consumed during a test and the sum of the power consumed. These measurements will be useful in the optimization of the simultaneous roughing operation.

The location of the power meter is away from the machining, thus consistent reliable measurements are expected from this sensor. The power meter was bolted to the metal wall inside the electrical breaker cabinet of the lathe. The cables which connect the breaker switch to the rest of the lathe's electromechanical systems were routed through the three toroidal Hall Effect sensors of the meter, and then reconnected to the breaker switch using terminal lugs. The power meter installed in the lathe is shown on Figure 3-10.

Figure 3-10: Power Meter mounted on lathe

The power meter data was sampled at 20 kHz. The data from the power meter was captured via a 2-conductor shielded wire and was connected to a National Instruments BNC shielded connector block.

3.1.8 Microphone

To monitor the audible sounds emitted from the machining process a Samson Audio Q8 dynamic microphone was used. The microphone is one of the most powerful tools used to determine chatter and irregularities in the machining process. To properly monitor the simultaneous cutting process the microphone was installed on the top of the lathe. A hole was drilled on the top of the lathe, directly above the work piece. The microphone installation can be seen in Figure 3-11.

Figure 3-11: (Left) Interior view of microphone (Right) Exterior view of microphone

All of the audible frequencies up to 20 kHz are of interest so the sampling rate chosen for the microphone was 40 kHz. The output from the microphone was routed via a BNC cable to a National Instruments BNC connector block.

3.1.9 Video Camera

A video capture of each experiment provides the experimenters with a visual and audible recording of what occurred during a certain experiment. This data can be tied to occurrences in nearly all of the sensors. A Flip Mino camera was used to record each experiment. The camera was mounted on the tailstock of the lathe through a magnetic adapter built specifically for this application. A screenshot of a video from a machining operation is seen on Figure 3-12.

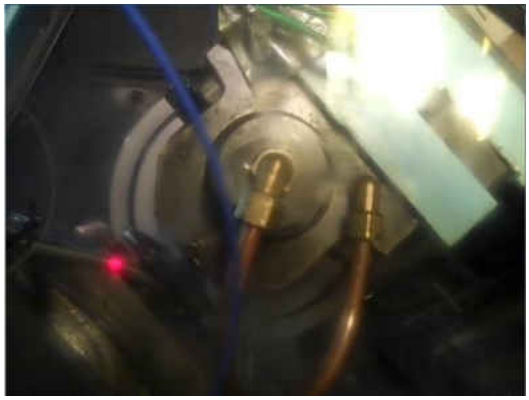

Figure 3-12: Screenshot of Simultaneous machining by Flip camera

3.1.10 Microscope

One of the most important areas in this research is the ability to measure tool wear and tool life. The tool wear and tool life for this application was measured like most turning and boring operations are which is through the tool's flank wear. To measure the flank wear, a Dino-Lite Pro microscope was used along with the software provided by the company to measure the flank wear. The flank wear was measured at a magnification of 200x. This microscope is connected to the PC via a USB connection. A picture of the microscope and sample tool wear picture can be seen in Figure 3-13.

Figure 3-13: (Left) Dino Lite microscope (Right) Flank wear region for Test 138 OD tool

3.2 Data Acquisition Setup

To acquire data simultaneously from the sensors, National Instruments data acquisition hardware and LabView software was used. The data acquisition setup was designed to be as economical as possible while still powerful enough to capture the data simultaneously. The chassis chosen to capture the data was a NI PXI-1042 8 slot chassis. Six slots of chassis were used for cards and two of them were used for the CPU and hard drive.

The data acquisition cards were chosen according to the sensor sampling rates because sensors connected to the same card require the same sampling rate. Two separate PXI-6259 cards with a capability of measuring 1.25 MS/s were used for the AE sensors. These cards were placed in slots 1 and 2 of the PXI chassis and were sampled at 800 kHz. Three PXI-6220 sampling cards with a capability of measuring 250 KS/s were placed in slots 3, 4, and 5. The only sensor sampling data at 40 kHz is the microphone so slot 3 was dedicated solely to the microphone. Slot 4 was dedicated to the dynamometer and force sensors. Each one of these sensors has three signals representing each axis so a total of six channels were used. The last PXI-6220 card was used for the sensors sampling at 10 Hz. This includes the OD thermocouple, ID thermocouple,

metalworking fluid thermocouple, and metal working fluid flow meter. In slot 6 of the chassis a simultaneous sampling card was used. The simultaneous sampling card allows the user the capability to sample each channel simultaneously at 500 kS/s per channel. The two tri-axial accelerometers were sampled on this card. The complete data acquisition setup can be seen on Figure 3-14.

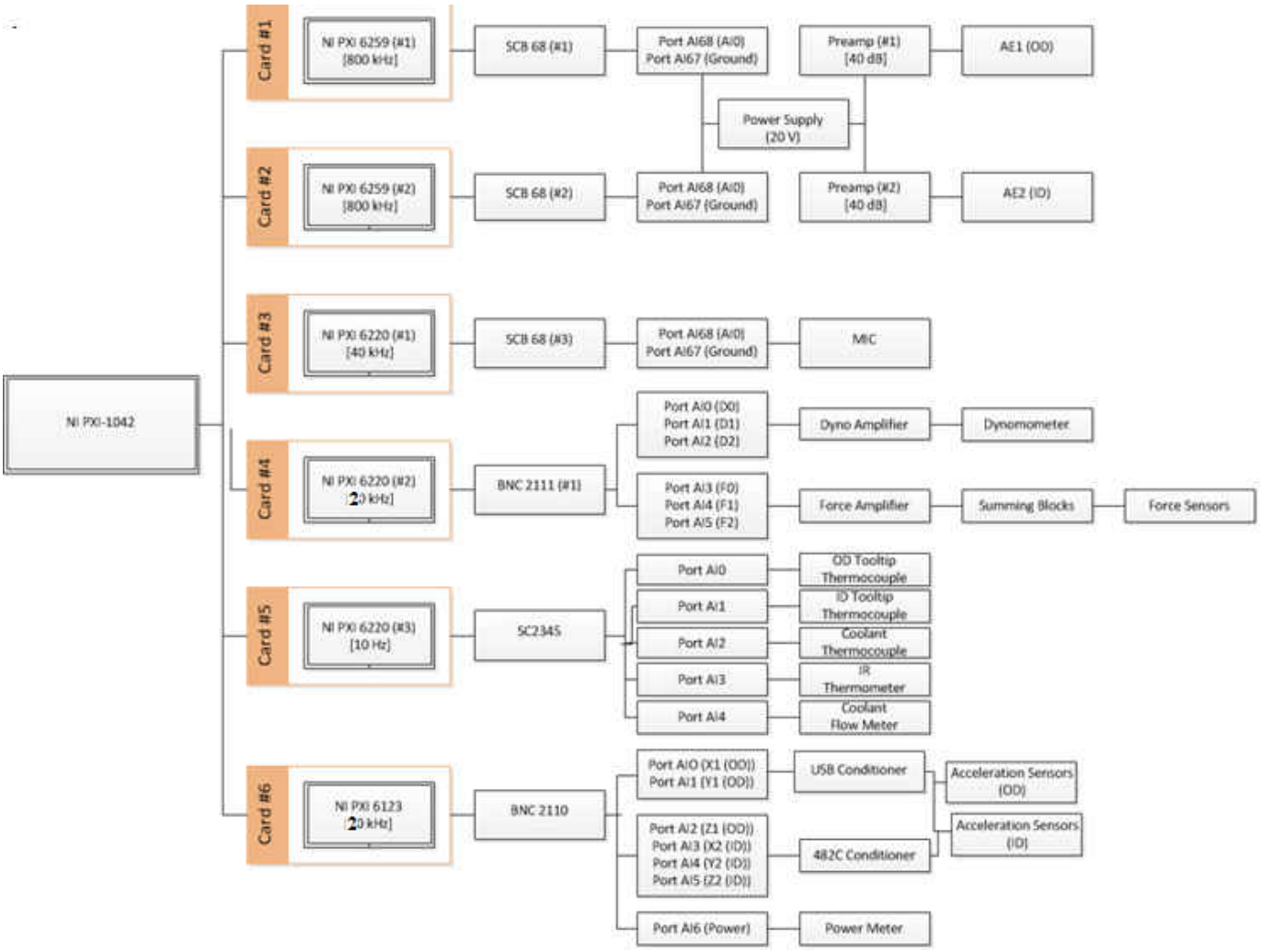

Figure 3-14: Data Acquisition Diagram

To record the data simultaneously, a program was created in LabView software. The architecture behind the program design was a producer/consumer loop. The producer/consumer loop is efficient when sampling data from various cards at different sampling rates. The methodology behind the producer/consumer loop is efficient yet simple. There are simply loops that produce data and loops that consume or write the data. The production of data is much faster than the writing of the data so buffering of the data must occur before it is written in the hard drive.

The file format used for recording the data was a .tdms file. The .tdms file allows for fast recording speeds by storing the memory to an array of 32-bit unsigned integers. A detriment to using this file format is that it requires scaling of the data after the experiment was performed. This required for the creation of another program to scale the data.

Another program was created to extract the data and gather all of the metrics necessary for the analysis. The data recorded from the producer/consumer loop program is triggered by a button and is stopped by a different button programmed in the LabView interface. The data of interest is during the steady portion of the roughing pass. The second program performed the function of scaling the data and then determining the steady state conditions from a slope finding algorithm. The slope finding algorithm was tuned to determine the steady state condition by searching for large changes in the slope of the time domain data of the power meter. After the steady state power data is found, then the signal is chunked to only the steady portion. The rest of the sensors are also chunked in the same region that the power data was chunked. From all of the chunked data, the statistical metrics were gathered for the Response Surface analysis. Also FFT

plots were generated from the chunked data. A diagram of the methodology behind the data extraction program is seen in Figure 3-15.

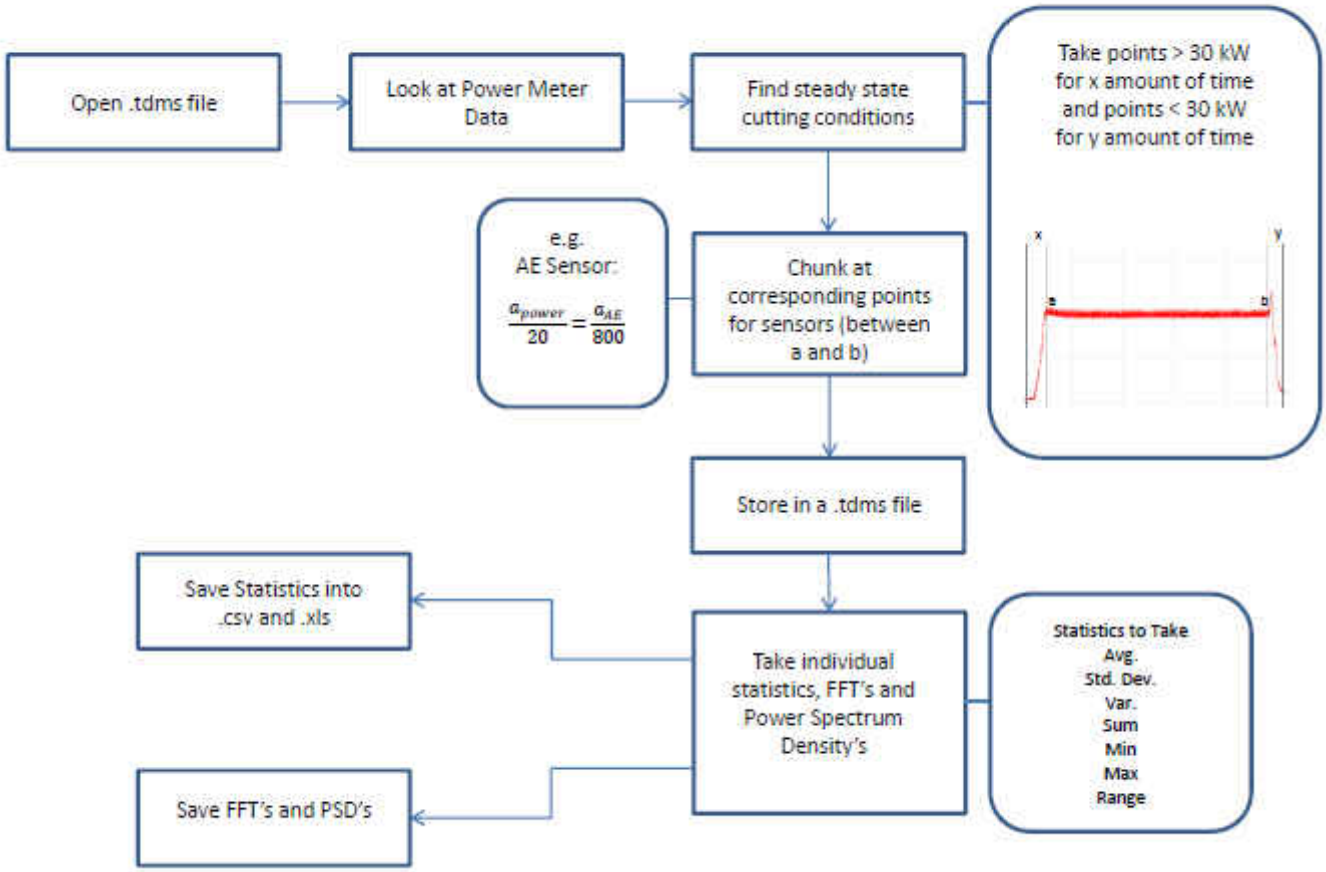

Figure 3-15: Diagram of Data Extraction Program

The main data analyzed in this research are the statistical metrics from the tests. After each test was performed the data was stored in the PXI chassis. The data was then carried to a PC used in the lab to be scaled and extract the metrics needed. The statistics gathered were stored in an Excel file and were then copied to Minitab 16.

3.3 Design of experiments

A total of four sets of experiments were run to model and optimize the simultaneous machining operation. The experimental phase began with the screening stage using a factorial design to determine if the chosen cutting conditions were feasible. The second set of experiments was called Response Surface I (RSI) in which a face centered Central Composite Design was used to monitor the responses at the chosen factor levels. In RSI, the work piece was pre-machined to a known diameter and then the experiment was performed. The motive behind the machining was to minimize the variation in the models. After the completion of RSI, the same tool edge was used for each corresponding experimental design point in RSII and RSIII totaling three passes on each tool edge. RSII and RSIII emulated the machining performed at the Red Lion facility and is the focus of this research. The experimental design for RSII and RSIII was completely the same. The runs performed for RSII and RSIII are shown in Tables 3-1 and 3-2.

Table 3-1: Design of experiments for RSII

Run Order	Point Type	Block	Spindle Speed (rpm)	Feed rate (in/rev)	OD DOC (in)	ID DOC (in)	Test Number
1	1	4	280	0.016	0.120	0.200	131
2	1	4	420	0.016	0.200	0.200	132
3	1	4	280	0.016	0.200	0.120	133
4	1	4	420	0.024	0.200	0.120	134
5	0	4	350	0.020	0.160	0.160	135
6	1	4	280	0.024	0.200	0.200	136
7	0	4	350	0.020	0.160	0.160	137
8	1	4	420	0.016	0.120	0.120	138
9	1	4	280	0.024	0.120	0.120	139
10	1	4	420	0.024	0.120	0.200	140
11	1	5	420	0.024	0.200	0.200	141
12	0	5	350	0.020	0.160	0.160	142
13	1	5	420	0.016	0.200	0.120	143
14	1	5	280	0.016	0.120	0.120	144
15	1	5	280	0.016	0.200	0.200	145
16	1	5	280	0.024	0.200	0.120	146
17	1	5	420	0.024	0.120	0.120	147
18	0	5	350	0.020	0.160	0.160	148
19	1	5	280	0.024	0.120	0.200	149
20	1	5	420	0.016	0.120	0.200	150
21	-1	6	350	0.020	0.160	0.200	151
22	-1	6	350	0.020	0.200	0.160	152
23	-1	6	350	0.016	0.160	0.160	153
24	0	6	350	0.020	0.160	0.160	154
25	-1	6	420	0.020	0.160	0.160	155
26	-1	6	350	0.024	0.160	0.160	156
27	-1	6	350	0.020	0.120	0.160	157
28	0	6	350	0.020	0.160	0.160	158
29	-1	6	350	0.020	0.160	0.120	159
30	-1	6	280	0.020	0.160	0.160	160
31	0	6	350	0.020	0.160	0.160	161

Table 3-2: Design of experiments for RSIII

Run Order	Pt Type	Block	Spindle Speed (rpm)	Feed rate (in/rev)	OD DOC (in)	ID DOC (in)	Test Number
1	1	7	280	0.016	0.120	0.120	162
2	1	7	420	0.024	0.120	0.120	163
3	0	7	350	0.020	0.160	0.160	164
4	1	7	280	0.016	0.200	0.200	165
5	1	7	280	0.024	0.120	0.200	166
6	0	7	350	0.020	0.160	0.160	167
7	1	7	420	0.016	0.200	0.120	168
8	1	7	280	0.024	0.200	0.120	169
9	1	7	420	0.016	0.120	0.200	170
10	1	7	420	0.024	0.200	0.200	171
11	0	8	350	0.020	0.160	0.160	172
12	1	8	280	0.016	0.120	0.200	173
13	1	8	280	0.024	0.200	0.200	174
14	1	8	420	0.016	0.120	0.120	175
15	1	8	280	0.024	0.120	0.120	176
16	1	8	420	0.024	0.200	0.120	177
17	1	8	420	0.016	0.200	0.200	178
18	1	8	280	0.016	0.200	0.120	179
19	0	8	350	0.020	0.160	0.160	180
20	1	8	420	0.024	0.120	0.200	181
21	0	9	350	0.020	0.160	0.160	182
22	-1	9	350	0.020	0.160	0.120	183
23	0	9	350	0.020	0.160	0.160	184
24	-1	9	350	0.024	0.160	0.160	185
25	-1	9	350	0.020	0.160	0.200	186
26	-1	9	280	0.020	0.160	0.160	187
27	-1	9	350	0.016	0.160	0.160	188
28	-1	9	350	0.020	0.200	0.160	189
29	-1	9	420	0.020	0.160	0.160	190
30	-1	9	350	0.020	0.120	0.160	191

Each row of Tables 3-1 and 3-2 represents a design point. The Run Order column is simply the order in which the experiments were performed. The Point Type column represents what type of test was performed by a 1, 0 or -1. If the Point Type column has a number 1 in the row then the test represents a corner point of the experimental design cube. The number 0 represents a centerpoint test and a 1 represents an axial run. Each set of experiments is broken up into blocks which allows for analysis of each of block to determine if the separation into blocks has an effect on the results. This requires sacrificing a degree of freedom for each block but the if the block has no effect then the degrees of freedom can be replaced and used to estimate for lack of fit. All of the four factors and variations of the factor levels are shown under the Spindle Speed, Feed rate, OD DOC and ID DOC columns. The last column represents the given test number.

4 CHAPTER 4 – EXPERIMENTAL RESULTS

4.1 Response Surface Modeling

To represent the simultaneous roughing operation, ten different responses were chosen carefully among all of the responses gathered. The responses chosen to represent the simultaneous removal operation included force, temperature, power, time, wear and cost models. Since the application of this research is focused towards emulating the Red Lion facility conditions, RSI is only used as a basis to determine how the responses were to be modeled under near perfect cutting conditions. In this section of the chapter, the final models for the chosen responses will be described in detail.

The main sets of models were derived from the RSII experiments which used the work pieces that had no previous machining performed in order to mirror the Red Lion facility. These models were compared with the responses in RSIII to ensure that the results gathered were accurate. Since RSII and RSIII are replicates using different work pieces, comparing the sets of experiments will verify if the models created are truly accurate. Since the same tool edge is used for each experimental point a slight change in the models from RSII to RSIII is expected as the wear increases slightly. Since the wear increases more at higher operating conditions, the models are expected to deviate more at higher operating conditions (i.e increased spindle speeds and feed rates).

The equations for each of the models will be presented. Each of the four factors were assigned a variable: x_1 = Spindle Speed, x_2 = Feed rate, x_3 = OD Depth of Cut, and x_4 = ID

Depth of Cut. The individual test results for each Response Surface set of experiments is shown in Appendix A and Appendix B.

4.1.1 Cut Time Model

The cut time plays the largest role in the optimization of the simultaneous cutting operation as producing parts faster will reduce the general costs of the facility. The final cut time model was driven by a combination of the spindle speed, and feed rate factors. This is expected as the depth of cut has no impact on how fast the work piece is cut. The final model required 5 degrees of freedom for the calculation of the model thus leaving 25 degrees of freedom for calculation of error. Table 4-1, shows the analysis of variance performed for the model. The least contribution to the model is made by the f^2 term.

Table 4-1: Analysis of Variance of the Cut Time Model

Source	**D.O.F**	**Seq SS**	**Adj SS**	**Adj MS**	**F**	**P**
Regression	5	3351.590	3351.590	670.320	696.990	0.000
Linear	2	3222.370	3222.370	1611.180	1675.280	0.000
Speed	1	1552.170	1552.170	1552.170	1613.920	0.000
Feed	1	1670.200	1670.200	1670.200	1736.650	0.000
Square	2	101.690	101.690	50.850	52.870	0.000
Speed*Speed	1	94.190	20.850	20.850	21.680	0.000
Feed*Feed	1	7.500	7.500	7.500	7.800	0.010
Interaction	1	27.530	27.530	27.530	28.630	0.000
Speed*Feed	1	27.530	27.530	27.530	28.630	0.000
Residual Error	25	24.040	24.040	0.960		
Lack-of-Fit	3	0.920	0.920	0.310	0.290	0.831
Pure Error	22	23.120	23.120	1.050		
Total	30	3375.640				

The regression applied to the cut time model using the two factors chosen, yielded an R-Sq. value of 99.29% with a standard deviation of 0.980682 s. The equation for cut time is shown in Equation 4.1. The cut time model shows that within the experimental region, each test ranged between 28 and 65 s. The approximate time for this experiment at Red Lion conditions would be 41.87 s. In order to speed up the cut time both the feed rate and the spindle speed must be increased.

$$\begin{aligned} Cut\ Time(s) = {} & 267.300 - 0.576570 \times x_1 - 7724.24 \times x_2 + 0.0005003 \times x_1^2 + 91909.9 \times x_2^2 \\ & + 4.68478 \times x_1 \times x_2 \end{aligned} \tag{4.1}$$

The cut time equation can be plotted to show how each one of the factors affects the time. The plot of the cut time equation can be seen in Figure 4-1. As expected, the results yielded a minimal cutting time at a high spindle speed and feed rate.

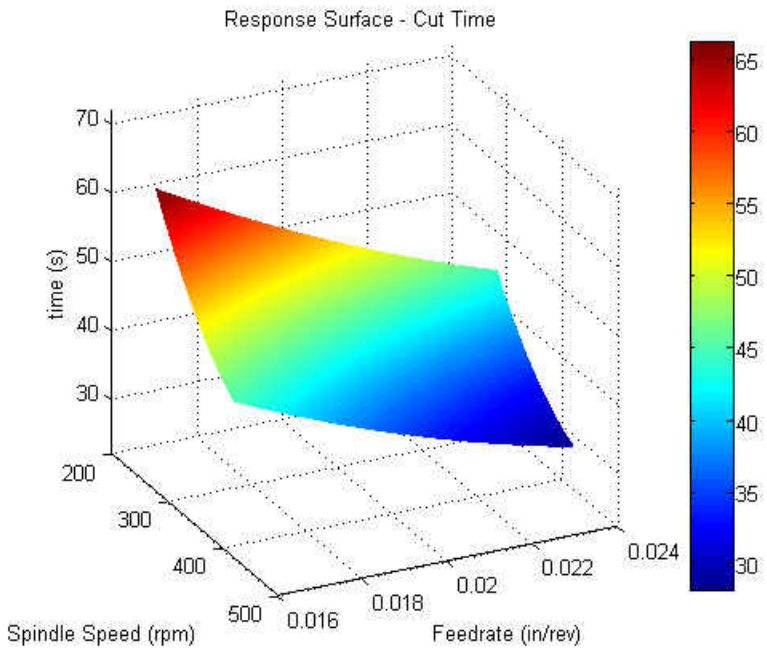

Figure 4-1: Surface Plot of the Cut Time Model

When compared with RSIII at various different locations, it is seen that the models are nearly the same. A comparison between the RSII and RSIII models can be seen in Table 4-3.

Table 4-2: Comparison of Cut Time Model between RSII and RSIII

Model Point	**Spindle Speed (rpm)**	**Feed rate (in/rev)**	**RSII - Cut Time (s)**	**RSIII - Cut Time (s)**	**Percent Error (%)**
1	325	0.018	52.378	52.414	-0.070%
2	350	0.020	41.861	41.766	0.227%
3	375	0.023	33.704	34.007	-0.890%

4.1.2 Average Power Model

The average power is of importance in the optimization because if reducing power consumption in the facility is of interest, a statistical model can provide what factors need to be

reduced without hindering production. Also, it is important to stay within range of the operating conditions of the CNC Lathe. This lathe's main spindle drive motor has a capability of running 37 kW continuously and 45 kW for a 30 min. period of time. It is important to note that this is just the spindle motor and not the total power consumption of the lathe which was what was measured. The average power model derived from RSII yielded that the power was a function driven by all four factors. From the analysis of variance performed, the spindle speed was the factor that had the greatest impact on the power consumption of the lathe. Since the regression consumed 9 degrees of freedom, 21 were left to account for error. From the model accuracy, no more points are required to test the system for error. The analysis of variance performed for the average power model can be seen in Table 4-3.

Table 4-3: Analysis of Variance of the Average Power Model

Source	**D.O.F**	**Seq SS**	**Adj SS**	**Adj MS**	**F**	**P**
Regression	9	259933152.000	259933152.000	28881461.000	1262.760	0.000
Linear	4	252451627.000	252451627.000	63112907.000	2759.430	0.000
Speed	1	95133602.000	95133602.000	95133602.000	4159.440	0.000
Feed	1	74823100.000	74823100.000	74823100.000	3271.420	0.000
DOC OD	1	68516451.000	68516451.000	68516451.000	2995.680	0.000
DOC ID	1	13978474.000	13978474.000	13978474.000	611.170	0.000
Interaction	5	7481525.000	7481525.000	1496305.000	65.420	0.000
Speed*Feed	1	2053177.000	2053177.000	2053177.000	89.770	0.000
Speed*DOC OD	1	2831866.000	2831866.000	2831866.000	123.820	0.000
Speed*DOC ID	1	435822.000	435822.000	435822.000	19.060	0.000
Feed*DOC OD	1	2088922.000	2088922.000	2088922.000	91.330	0.000
Feed*DOC ID	1	71737.000	71737.000	71737.000	3.140	0.091
Residual Error	21	480307.000	480307.000	22872.000		
Lack-of-Fit	15	368089.000	368089.000	24539.000	1.310	0.389
Pure Error	6	112217.000	112217.000	18703.000		
Total	30	260413458.000				

The multiple linear regression model can predict the average power with an R-Sq. value of 99.82%. The standard deviation of the power is 151.234 W which seems large but when machining the lathe consumes on average more than 30 kW. From the analysis of variance it can also be seen that the OD depth of cut has a much larger effect in the power consumed in the operation simply due to its higher material removal rate. Although the depths of cut have a great impact on the model, the spindle speed and the feed rate still dominate the average power consumed in the operation. It is important to note that the final model did not yield any squared terms or interaction between the depths of cut. The final equation for average power consumption during the operation can be seen in Equation 4.2.

$$\begin{aligned} Average\,Power\,(W) = {} & 33004.5 - 26.2163 \times x_1 - 366357 \times x_2 - 48978.5 \times x_3 - 6969.23 \times x_4 + \\ & 1279.37 \times x_3 \times x_4 + 150.251 \times x_1 \times x_3 + 58.9436 \times x_1 \times x_4 + \\ & 225829 \times x_2 \times x_3 + 418497 \times x_2 \times x_4 \end{aligned} \tag{4.2}$$

The response surface for the power is a function of more than two factors thus it cannot be shown in a surface plot. To demonstrate how the average power affected each of the coefficients a combined contour plot is shown in Figure 4-2. From this plot it can be seen that the spindle speed vs. feed rate diagram, shows the largest change in average power. It can also be seen that the plots that include the ID depths of cut provide very little curvature.

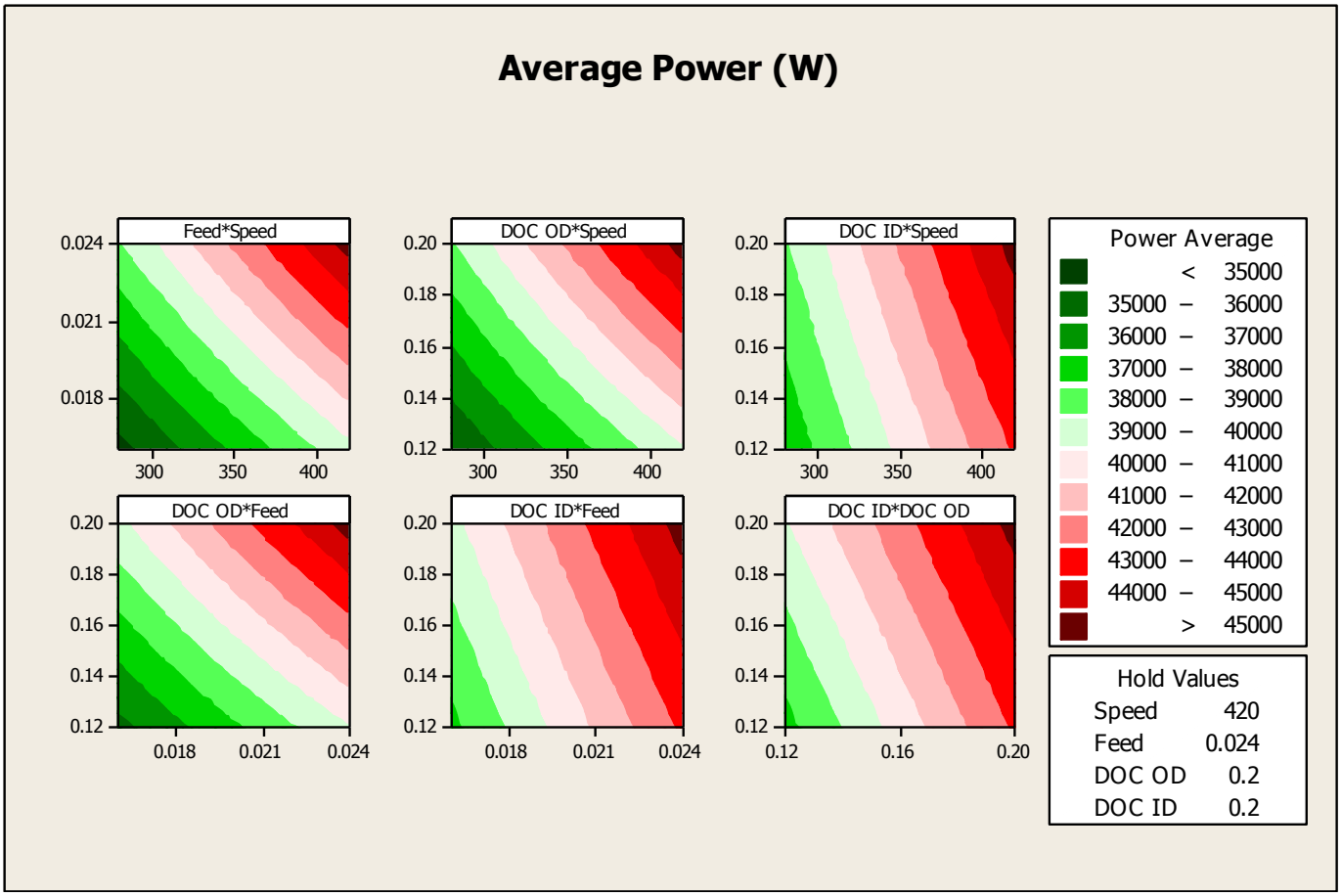

Figure 4-2: Contour Plots of the Average Power Model

The average power was compared to RSIII at the same points as the Cut Time model. The results from the comparison can be seen in in Table 4-4. Since the Cut Time model did not include the depths of cut, depths of cut were chosen randomly to compare results. The differences between the RSII and RSIII are minimal thus ensuring that the results are accurate within the chosen experimental region. The increase in power from RSII to RSIII is evident due to the extra amount of power required to perform the operation after the tool wear has increasing by the added pass.

Table 4-4: Comparison of the Average Power Model between RSII and RSIII

Model Point	Spindle Speed (rpm)	Feed rate (in/rev)	OD DOC (in)	ID DOC (in)	RSII - Avg. Power (W)	RSIII - Avg. Power (W)	Percent Error (%)
1	325	0.018	0.150	0.170	34572.259	34584.100	0.034%
2	350	0.020	0.130	0.140	34882.371	34954.025	0.205%
3	375	0.023	0.170	0.190	40279.838	40284.521	0.012%

4.1.3 Power Sum Model

The average power is important when determining what factors will reduce the power consumption during machining, but does not take into account on how long the machining process took to complete. The sum of the power was measured in order to visualize the amount of power consumed throughout an entire test. The power sum was measured by summing the amount of Watts consumed from the beginning of the cut until the cut was completed. Since this metric would yield such a large value, the end result was divided by 10^{10}. The model created for the power sum consisted of all factors, but second order terms only consisted of the Spindle Speed and Feed rate factors. The analysis of variance is shown in Table 4-5.

Table 4-5: Analysis of Variance of the Power Sum Model

Source	D.O.F	Seq SS	Adj SS	Adj MS	F	P
Regression	7	9.730	9.730	1.390	310.790	0.000
Linear	4	9.401	9.401	2.350	525.490	0.000
Speed	1	4.010	4.010	4.010	896.630	0.000
Feed	1	4.921	4.921	4.921	1100.220	0.000
DOC OD	1	0.340	0.340	0.340	75.940	0.000
DOC ID	1	0.131	0.131	0.131	29.190	0.000
Square	2	0.292	0.292	0.146	32.690	0.000
Speed*Speed	1	0.269	0.057	0.057	12.740	0.002
Feed*Feed	1	0.024	0.024	0.024	5.270	0.031
Interaction	1	0.037	0.037	0.037	8.160	0.009
Speed*Feed	1	0.037	0.037	0.037	8.160	0.009
Residual Error	23	0.103	0.103	0.004		
Lack-of-Fit	17	0.062	0.062	0.004	0.540	0.851
Pure Error	6	0.041	0.041	0.007		
Total	30	9.833				

From the analysis of variance, it can be seen that the regression accounted for 7 degrees of freedom, leaving 23 degrees of freedom to estimate for error. The linear terms of the Spindle Speed and the Feed rate accounted for 90.8% of the total model. The Power Sum can be estimated with an R-Sq. value of 98.95% and a standard deviation of 0.0668760 W. The equation for the Power Sum model is shown in Equation 4.3.

$$\frac{PowerSum}{10^{10}}(W) = 13.6185 - 0.0284610 \times x_1 - 396.470 \times x_2 + 3.43396 \times x_3 + 2.12904 \times x_4 + 2.61521E\text{-}05 \times x_1^2 + 5151.33 \times x_2^2 + 0.170586 \times x_1 \times x_2 \quad (4.3)$$

The response surface for the Power Sum model was plotted similarly to the Average Power model and it is shown in Figure 4-3. From this plot the influence of the combination of

Spindle Speed and Feed rate can clearly be seen. The faster the cut is performed, the lower the total power consumption for a test. A general trend can be seen in increasing total power as the depths of cut are increased.

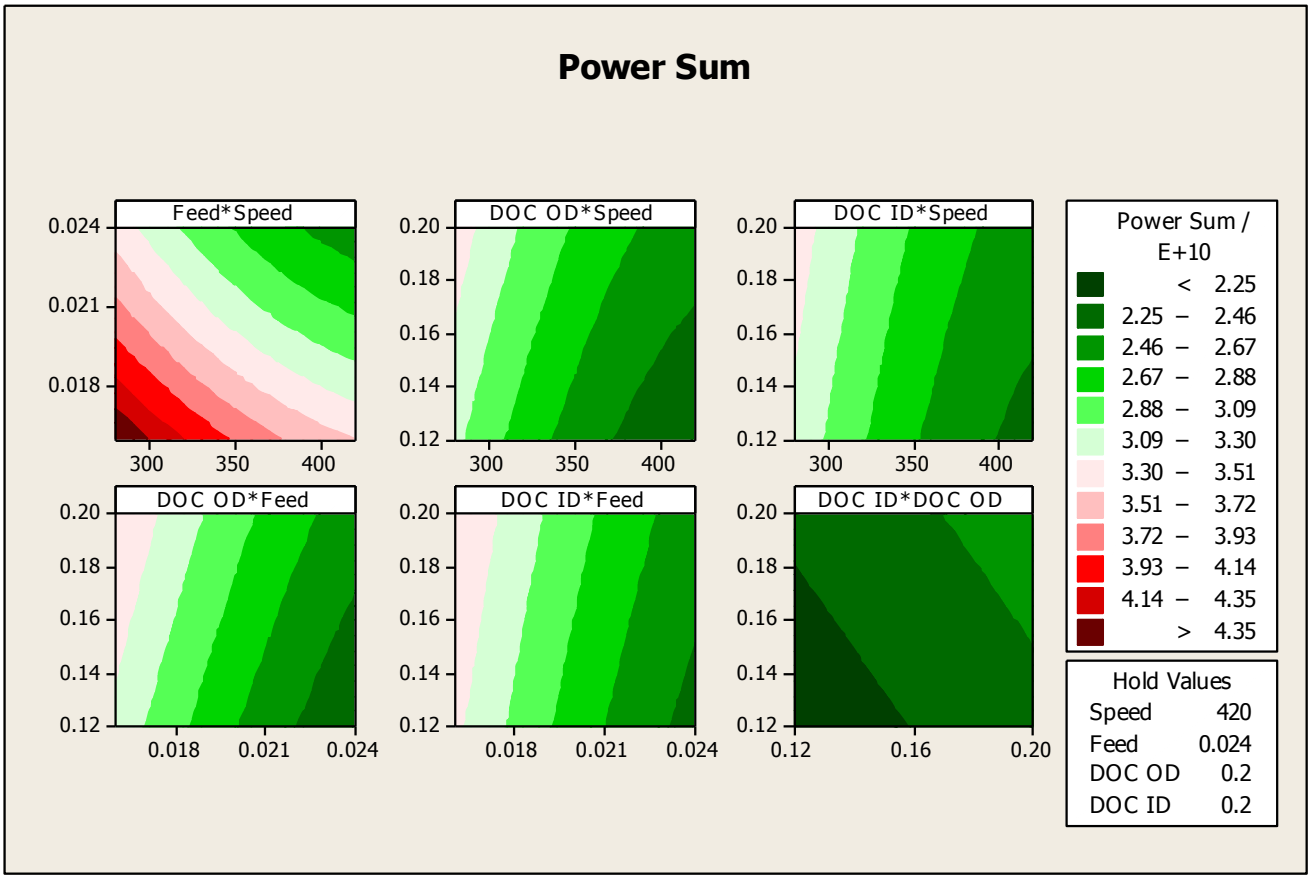

Figure 4-3: Contour Plots of the Power Sum Model

The results from the Power Sum model obtained from RSII were compared to the RSIII model at the same points as the Average Power Model. The results in the comparison can be seen in Table 4-6. From the points tested a slight amount of error increase can be seen as all of the factors are increased.

Table 4-6: Comparison of the Power Sum Model between RSII and RSIII

Model Point	Spindle Speed (rpm)	Feed rate (in/rev)	OD DOC (in)	ID DOC (in)	RSII - Power Sum/E+10 (W)	RSIII - Power Sum/E+10 (W)	Percent Error (%)
1	325	0.018	0.150	0.170	3.618	3.618	-0.023%
2	350	0.020	0.130	0.140	2.930	2.927	0.106%
3	375	0.023	0.170	0.190	2.738	2.781	-1.525%

4.1.4 OD Feed Force Model

From the set of tool life experiments performed it was determined that the feed force was prone to increase the most as the tool wear increased for this operation. From these results it was decided that out of the three forces measured, the feed force would be used as the representative force in the optimization model. The feed force was measured by the Y-axis of the dynamometer and was a function of the feed rate and depth of cut. From basic turning theory it is important to note that the Response Surface model for the OD feed force is very close to the traditional cutting force model which is a function of the specific cutting and the chip area. The chip areas is a function of the feed rate and depth of cut. Although the feed rate has significant impact on the force, the OD depth of cut generally has the most impact on the response. The analysis of variance for the OD feed force is shown in Table 4-7.

Table 4-7: Analysis of Variance of the OD Feed Force Model

Source	D.O.F	Seq SS	Adj SS	Adj MS	F	P
Regression	4	7219234.000	7219234.000	1804809.000	123.180	0.000
Linear	2	6910223.000	6588952.000	3294476.000	224.860	0.000
Feed	1	1321229.000	2095316.000	2095316.000	143.010	0.000
DOC OD	1	5588994.000	5453498.000	5453498.000	372.220	0.000
Square	1	190328.000	152905.000	152905.000	10.440	0.004
DOC OD*DOC OD	1	190328.000	152905.000	152905.000	10.440	0.004
Interaction	1	118683.000	118683.000	118683.000	8.100	0.009
Feed*DOC OD	1	118683.000	118683.000	118683.000	8.100	0.009
Residual Error	24	351631.000	351631.000	14651.000		
Lack-of-Fit	4	50792.000	50792.000	12698.000	0.840	0.514
Pure Error	20	300839.000	300839.000	15042.000		
Total	28	7570866.000				

The analysis of variance of the force model yielded 4 degrees of freedom dedicated to the regression and 24 degrees of freedom for error. The total degrees of freedom that every model should have are 30, but due to sensor errors two tests did not have force measurements. The tests could not be repeated because the same tool edge is used for every test using the same settings thus another pass on the tool would result in inaccurate RSIII data. The OD feed force could be predicted with an R-Sq. value of 95.36% and a standard deviation of 121.043 N. The equation for force is shown in Equation 4.4.

$$OD\ Feed\ Force(N) = -2165.36 - 1911.73 \times x_2 + 32827.0 \times x_3 - 92700.8 * \times x_3^2 + 597176 \times x_2 \times x_3 \quad (4.4)$$

The surface plot for the OD feed force is shown in Figure 4-4. The response surface of the OD Feed force corresponds to the model showing a much larger slope for increasing OD Depth of cut than for increasing feed rate.

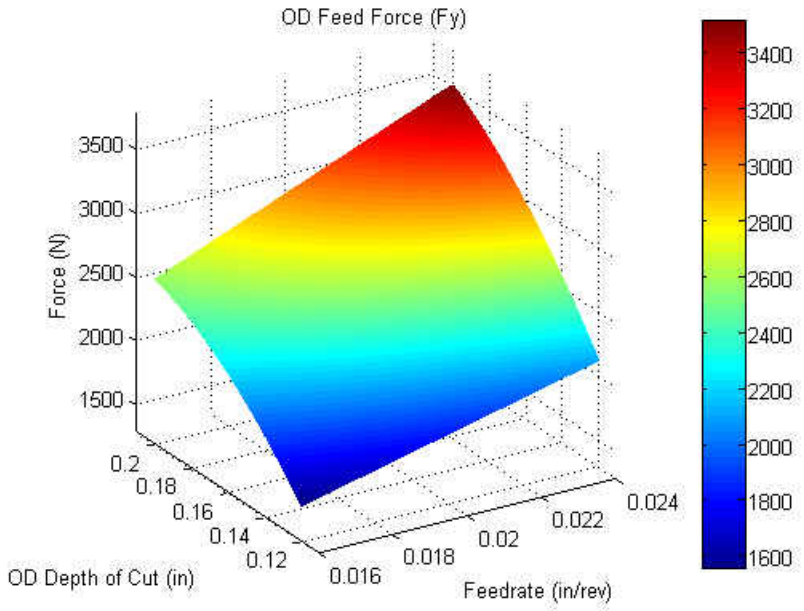

Figure 4-4: Surface Plot of the OD Feed Force Model

The results from RSII were compared to RSIII. The results for RSIII were surprisingly slightly lower than RSII. Although the results for RSIII are slightly lower, the change in the model is not great as the results are all close to within a standard deviation. For the third model point the results are nearly exactly the same indicating a very strong model in that region.

Table 4-8: Comparison of the OD Feed Force Model between RSII and RSIII

Model Point	Spindle Speed (rpm)	Feed rate (in/rev)	OD DOC (in)	ID DOC (in)	RSII -OD Feed Force (N)	RSIII - OD Feed Force (N)	Percent Error (%)
1	325	0.018	0.150	0.170	2207.054	2074.803	6.374%
2	350	0.020	0.130	0.140	2049.929	1952.958	4.965%
3	375	0.023	0.170	0.190	2977.361	2976.275	0.036%

4.1.5 ID Feed Force Model

The ID feed force was measured by the X-axis of the force sensors. Similar to the OD feed force, the ID feed force was a function of the feed rate and the ID depth of cut. The ID depth of cut had the greatest impact on the feed force. The analysis of variance for the feed force model is show on Table 4-9.

Table 4-9: Analysis of Variance of ID Feed Force Model

Source	D.O.F	Seq SS	Adj SS	Adj MS	F	P
Regression	3	4150727.000	4150727.000	1383576.000	488.620	0.000
Linear	2	4120445.000	4120445.000	2060223.000	727.580	0.000
Feed	1	247519.000	247519.000	247519.000	87.410	0.000
DOC ID	1	3872926.000	3872926.000	3872926.000	1367.750	0.000
Interaction	1	30282.000	30282.000	30282.000	10.690	0.003
Feed*DOC ID	1	30282.000	30282.000	30282.000	10.690	0.003
Residual Error	26	73622.000	73622.000	2832.000		
Lack-of-Fit	5	13449.000	13449.000	2690.000	0.940	0.476
Pure Error	21	60173.000	60173.000	2865.000		
Total	29	4224349.000				

From the analysis of variance it can be seen that only 29 degrees of freedom were used to build the model indicating that 1 degree of freedom was eliminated. This was due to a sensor

error during a centerpoint test. The centerpoint test will not affect the results as there are 5 more to estimate curvature towards the center of the experimental region. The force can be estimated with an R-Sq. value of 98.26% with a standard deviation of 53.2128 N. The standard deviation of the ID feed force is greater than half of the OD feed force. These results were unexpected as the inner diameter suffers from eccentricity. From the observed results, it can be defined that the feed force can still be measured accurately even with eccentric work pieces. The equation for the ID feed force was calculated and it is shown in Equation 4.5.

$$ID\ Feed\ Force(N) = 67.7811 - 14188.3 \times x_2 + 6158.34 \times x_4 + 271903 \times x_2 \times x_4 \quad (4.5)$$

The ID feed force model is different that the OD feed force model in the sense that it experiences very little curvature. In Figure 4-5, it can be seen that as the ID depth of cut increases, the feed force increases greatly. To minimize the force the federate and ID depth of cut must be minimized, but as will be seen in the ID tool wear model, these settings will not provide the least wear.

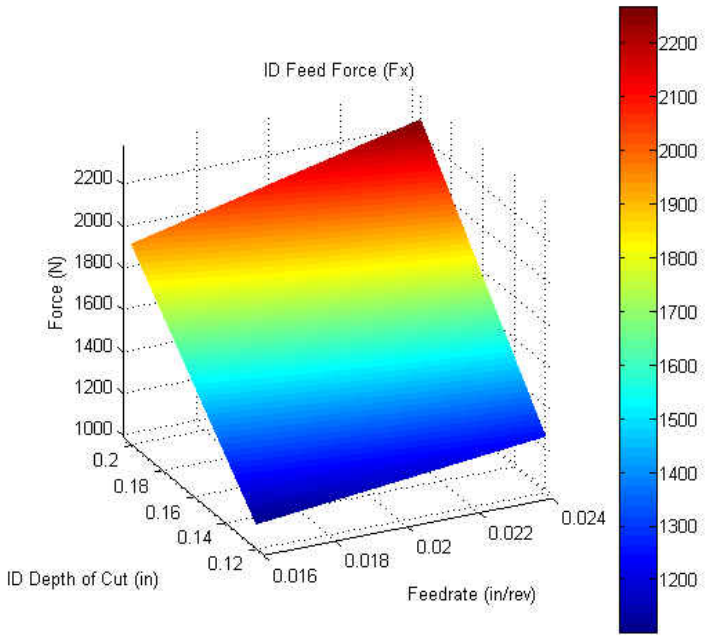

Figure 4-5: Surface Plot of ID Feed Force Model

The ID feed force RSII model was compared to the RSIII model. The results are shown on Table 4-10. It is clear that there is an increase in feed force from RSII to RSIII indicating wear progression on the tool from RSII to RSIII. The increase in force is between 4-5%.

Table 4-10: Comparison of the ID Feed Force Model between RSII and RSIII

Model Point	**Spindle Speed (rpm)**	**Feed rate (in/rev)**	**OD DOC (in)**	**ID DOC (in)**	**RSII - ID Feed Force (N)**	**RSIII - ID Feed Force (N)**	**Percent Error (%)**
1	325	0.018	0.150	0.170	1675.315	1745.402	-4.016%
2	350	0.020	0.130	0.140	1407.511	1495.852	-5.906%
3	375	0.023	0.170	0.190	2081.014	2183.953	-4.713%

4.1.6 OD Tool Temperature Model

The OD tool temperature was measured by the thermocouple on the shim of the tool. The position of the thermocouple is of great importance to the results, as a slight shift in the cable will measure temperature in a different region of the tool. Since the thermocouple tip protruded slightly beyond the outer edge of the shim, the thermocouple tip was often sheared by chips and was always under coolant wash. This greatly affected the accuracy of the results, as new thermocouples had to be installed. The results for the temperature indicated that the OD tool temperature was a function of the OD depth of cut and the Feed rate. The analysis of variance for the tool temperature is shown on Table 4-11.

Table 4-11: Analysis of Variance of the OD Tool Temperature Model

Source	**D.O.F**	**Seq SS**	**Adj SS**	**Adj MS**	**F**	**P**
Regression	3	21772.100	21772.100	7257.400	34.590	0.000
Linear	2	21290.400	21290.400	10645.200	50.730	0.000
Feed	1	4641.100	4641.100	4641.100	22.120	0.000
DOC OD	1	16649.300	16649.300	16649.300	79.350	0.000
Square	1	481.700	481.700	481.700	2.300	0.141
DOC OD*DOC OD	1	481.700	481.700	481.700	2.300	0.141
Residual Error	27	5665.300	5665.300	209.800		
Lack-of-Fit	5	508.200	508.200	101.600	0.430	0.820
Pure Error	22	5157.100	5157.100	234.400		
Total	30	27437.400				

From the analysis of variance, it can be seen that the OD depth of cut has the largest impact on the on the model, followed by the feed rate. The OD tool temperature was measured with an R-Sq. value of 79.35% with a standard deviation of 14.4854 ºF. The equation for the OD tool temperature can be seen in Equation 4.6.

$$OD\,Tool\,Temperature\,(F) = -149.786 + 4014.36 \times x_2 + 2358.02 \times x_3 - 4992.77 \times x_3^2 \quad (4.6)$$

The response for the OD tool temperature was very similar to force. The plot for the response can be seen in Figure 4-6.

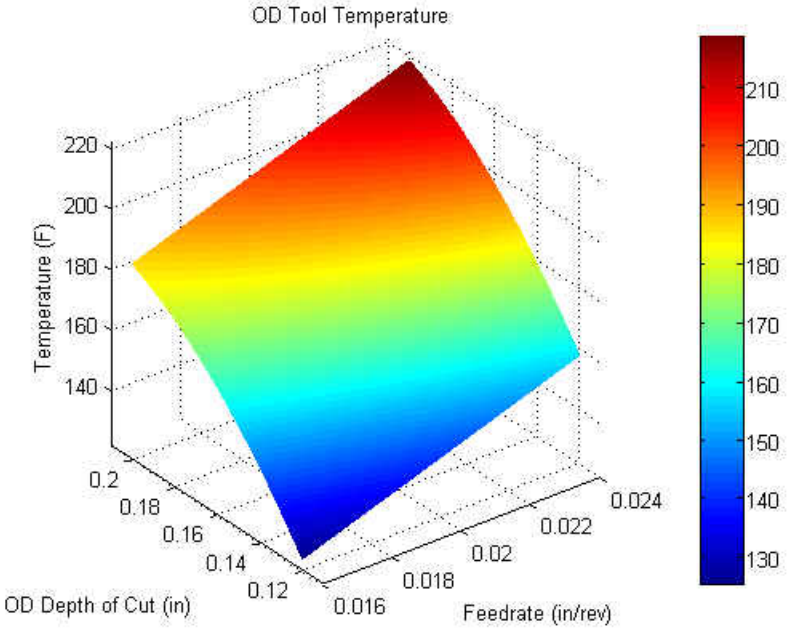

Figure 4-6: Surface Plot of the OD Tool Temperature Model

The results for the OD tool temperature were compared between RSII and RSIII and are shown on Table 4-12. All of the results were within a standard deviation indicating an accurate model. The tool life testing results did not indicate an increase in OD tool temperature as the tool wear progressed. This is evident in the comparison seen below.

Table 4-12: Comparison of the OD Tool Temperature Model between RSII and RSIII

Model Point	Spindle Speed (rpm)	Feed rate (in/rev)	OD DOC (in)	ID DOC (in)	RSII - OD Tool Temp (F)	RSIII - OD Tool Temp (F)	Percent Error (%)
1	325	0.018	0.150	0.170	161.831	167.207	-3.215%
2	350	0.020	0.130	0.140	152.666	156.733	-2.595%
3	375	0.023	0.170	0.190	197.109	188.351	4.650%

4.1.7 ID Tool Temperature Model

The ID thermocouple was mounted in the same way that the OD thermocouple was, thus suffered from the same environment. The main difference in the cutting environment between the OD and ID thermocouples is that the ID thermocouple was cutting inside of the work piece while coolant was flowing. The coolant flow flooded the ID thermocouple as it was trying to escape from the work piece as the tool was cutting. The ID tool temperature model was similar to the OD tool temperature model with the ID depth of cut being the most influential factor. The analysis of variance for the ID tool temperature is shown on Table 4-13.

Table 4-13: Analysis of Variance of the ID Tool Temperature Model

Source	D.O.F	Seq SS	Adj SS	Adj MS	F	P
Regression	3	6563.700	6563.700	2187.890	30.630	0.000
Linear	2	5750.200	5750.200	2875.100	40.250	0.000
Feed	1	639.000	639.000	638.980	8.950	0.006
DOC ID	1	5111.200	5111.200	5111.210	71.560	0.000
Square	1	813.500	813.500	813.480	11.390	0.002
Feed*Feed	1	813.500	813.500	813.480	11.390	0.002
Residual Error	27	1928.400	1928.400	71.420		
Lack-of-Fit	5	496.700	496.700	99.340	1.530	0.222
Pure Error	22	1431.700	1431.700	65.080		
Total	30	8492.100				

The ID tool temperature could be measured with an R-Sq. value of 77.29% with a standard deviation of 8.45125 ºF. The predictability of the ID and OD tool temperature are very similar but the standard deviation of the ID tool temperature is much lower indicating less variation of the ID tool temperature. The equation derived for the ID tool temperature is shown in Equation 4.7.

$$ID\,Tool\,Temperature\,(F) = 285.471 - 24463.3 \times x_2 + 421.275 \times x_4 + 648822 \times x_2^2 \quad (4.7)$$

The equation for the ID tool temperature was plotted and is shown in Figure 4-7. From this figure the curvature caused the second order feed term is evident. In order to reduce the temperature the feed rate must be near the center point region.

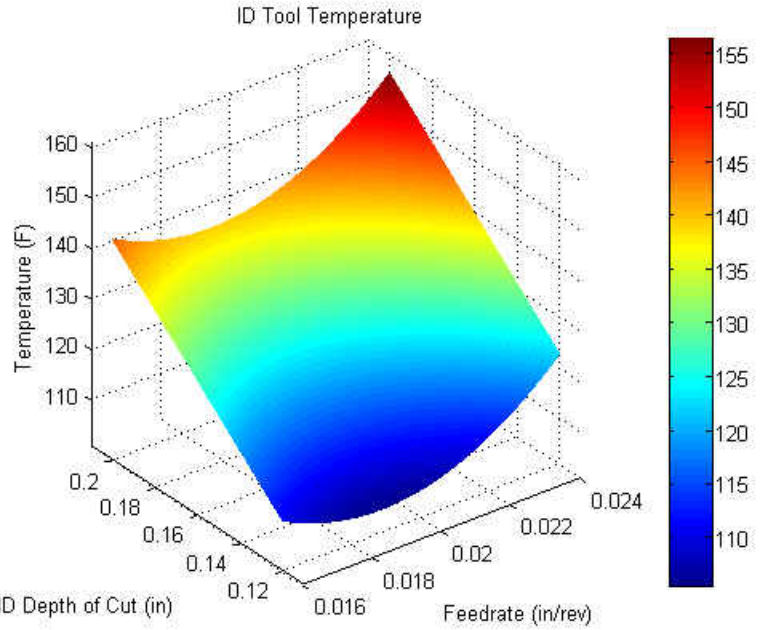

Figure 4-7: Surface plot of the ID Tool Temperature Model

The results between RSII and RSIII for the ID tool temperature yielded very similar results. The comparison between the two models is shown on Table 4-14.

Table 4-14: Comparison of the ID Tool Temperature Model between RSII and RSIII

Model Point	Spindle Speed (rpm)	Feed rate (in/rev)	OD DOC (in)	ID DOC (in)	RSII -ID Tool Temp (F)	RSIII -ID Tool Temp (F)	Percent Error (%)
1	325	0.018	0.150	0.170	127.682	127.272	0.322%
2	350	0.020	0.130	0.140	114.712	123.370	-7.017%
3	375	0.023	0.170	0.190	143.555	141.714	1.299%

4.1.8 OD Tool Wear Model

The OD tool wear was categorized by the flank wear measurement after eeach test. RSII models were categorized by the second pass on the tool edges and RSIII models were categorized by the third pass on the tool edges. The results from RSIII were expected to be more accurate than the RSII because as more passes are placed on the tool edge, the flank wear trend line appears clearer on the tool edge. The OD tool wear was a function of the spindle speed, feed rate and OD depth of cut. The OD tool wear is the first model described where a second order term has the largest influence on the response. The analysis of variance for the OD tool wear model is shown on Table 4-15.

Table 4-15: Analysis of Variance of the OD Tool Wear Model

Source	D.O.F	Seq SS	Adj SS	Adj MS	F	P
Regression	5	29182.000	29182.000	5836.400	14.840	0.000
Linear	3	13517.000	13517.000	4505.700	11.450	0.000
Speed	1	7914.000	7914.000	7914.000	20.120	0.000
Feed	1	1484.000	1484.000	1483.700	3.770	0.063
DOC OD	1	4119.000	4119.000	4119.300	10.470	0.003
Square	1	14506.000	14506.000	14505.900	36.880	0.000
Speed*Speed	1	14506.000	14506.000	14505.900	36.880	0.000
Interaction	1	1159.000	1159.000	1159.100	2.950	0.098
Speed*DOC OD	1	1159.000	1159.000	1159.100	2.950	0.098
Residual Error	25	9834.000	9834.000	393.400		
Lack-of-Fit	9	5617.000	5617.000	624.100	2.370	0.064
Pure Error	16	4217.000	4217.000	263.600		
Total	30	39016.000				

The analysis of variance for the OD tool wear models yields that the second order spindle speed term has the greatest influence on the model followed the by linear spindle speed term. The OD tool wear could be predicted with an R-sq. value of 74.79% with a standard deviation of 19.8334 microns. The equation for the OD tool wear is shown in Equation 4.8.

$$\begin{aligned} OD\,Tool\,Wear\,(\mu m) = {} & 1153.61 - 6.44933 \times x_1 + 2269.76 \times x_2 - 685.744 \times x_3 \\ & + 0.00894643 \times x_3^2 + 3.03982 \times x_1 \times x_3 \end{aligned} \quad (4.8)$$

Each one of the factors is compared to see how they affect the response in Figure 4-8. The second order effect of the spindle speed is evident when comparing the spindle speed with the feed rate and the OD depth of cut. More importantly it can be seen that when the spindle speed is maintained at lower levels the wear will minimal regardless of the OD depth of cut or the feed rate.

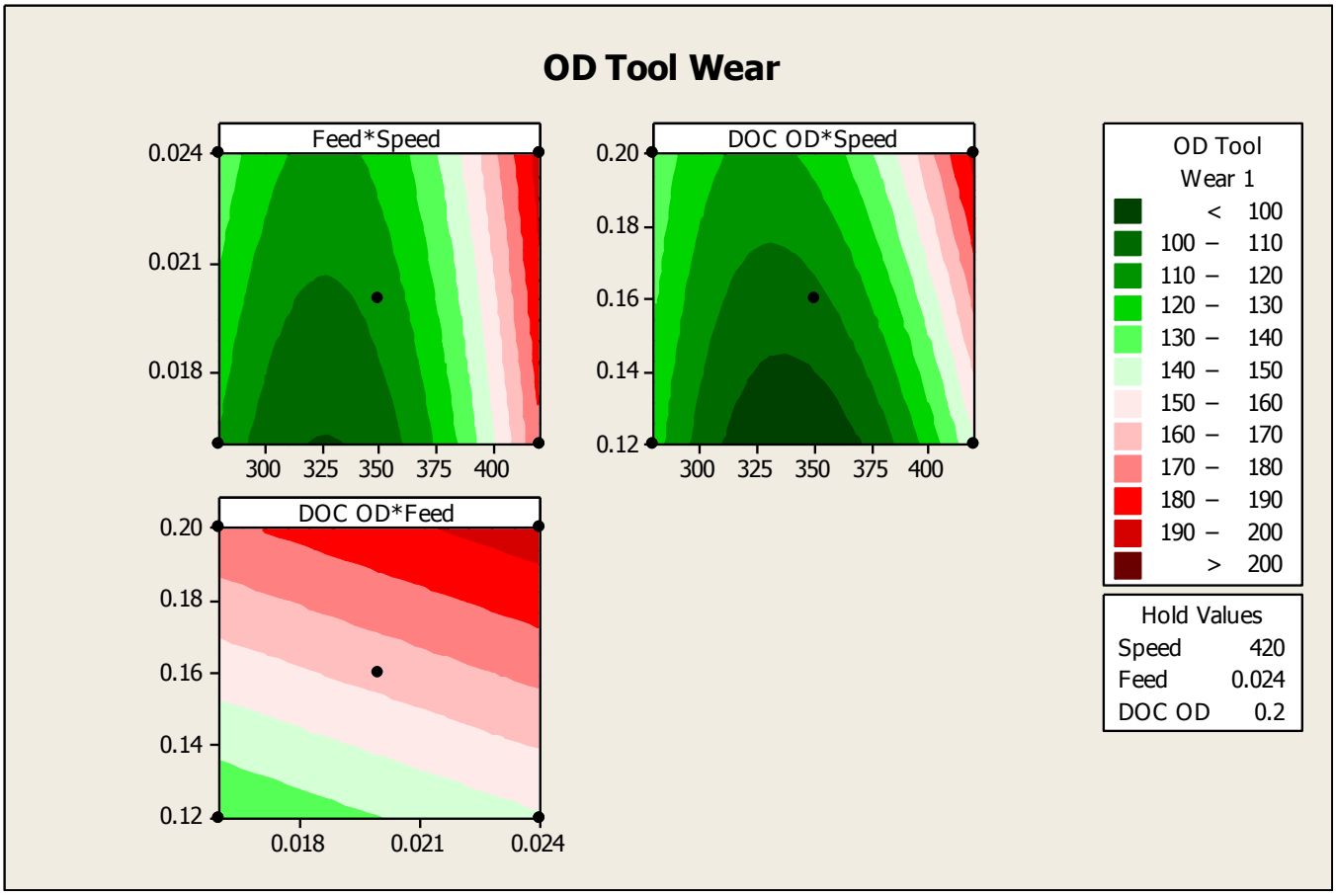

Figure 4-8: Contour Plots of the OD Tool Wear Model

The results from the OD tool wear model in RSII are compared to RSIII in Table 4-16. The increase in wear from one model to the other is evident, thus the models cannot be compared as to accuracy. The RSIII tool wear model was more accurate as the R-Sq. value changed to 90.23% due to a more defined wear line in each tool edge.

Table 4-16: Comparison of the OD Tool Wear Model between RSII and RSIII

Model Point	Spindle Speed (rpm)	Feed rate (in/rev)	OD DOC (in)	ID DOC (in)	RSII -OD Tool Wear (mm)	RSIII - OD Tool Wear (mm)	Percent Increase (%)
1	325	0.018	0.150	0.170	87.595	104.603	16.259%
2	350	0.020	0.130	0.140	86.842	105.161	17.420%
3	375	0.023	0.170	0.190	121.485	181.668	33.128%

4.1.9 ID Tool Wear Model

The ID tool wear was measured by measuring the flank wear on the tool edge after each test. Since the ID material removed is much less than the OD material removed the tool wear increases at a much slower pace. The ID Tool wear was a model defined by all of the factors. The OD depth of cut had an impact on the ID tool wear indicating that there is an interaction between the machining operation that affects the wear mechanism of the ID tool edge. Much like the OD tool wear model, the main contribution to the ID tool wear model was the second order spindle speed term followed by the linear speed term. The analysis of variance of the ID tool wear model is shown on Table 4-17.

Table 4-17: Analysis of Variance of the ID Tool Wear Model

Source	D.O.F	Seq SS	Adj SS	Adj MS	F	P
Regression	8	14929.600	14929.600	1866.200	6.470	0.000
Linear	4	3160.100	3160.100	790.020	2.740	0.056
Speed	1	2927.900	2927.900	2927.910	10.160	0.004
Feed	1	215.300	215.300	215.330	0.750	0.397
DOC OD	1	13.500	13.500	13.460	0.050	0.831
DOC ID	1	3.400	3.400	3.370	0.010	0.915
Square	1	5642.400	5642.400	5642.370	19.580	0.000
Speed*Speed	1	5642.400	5642.400	5642.370	19.580	0.000
Interaction	3	6127.100	6127.100	2042.370	7.090	0.002
Speed*Feed	1	2461.300	2461.300	2461.250	8.540	0.008
Speed*DOC OD	1	1916.200	1916.200	1916.210	6.650	0.018
Speed*DOC ID	1	1749.700	1749.700	1749.670	6.070	0.022
Error	21	6052.800	6052.800	288.230		
Lack-of-Fit	16	4306.700	4306.700	269.170	0.770	0.686
Pure Error	5	1746.100	1746.100	349.230		
Total	29	20982.400				

The ID tool wear model has an R-sq. value of 71.15% with a standard deviation of 16.9773 microns. One term was not counted in the model as the tool edge chipped during the pass. The equation for the ID tool wear is shown in Equation 4.9.

$$\begin{aligned} ID\,Tool\,Wear\,(\mu m) = {} & 1001.16 - 4.73064 \times x_1 - 14638.8 \times x_2 - 1389.57 \times x3 + \\ & 1296.35 \times x_4 + 0.00571306 \times x_1^2 + 44.2955 \times x_1 \times x_2 + \\ & 3.90844 \times x_1 \times x_3 - 3.73473 \times x_1 \times x_4 \end{aligned} \quad (4.9)$$

A contour plot was created to show how each one of the responses affected the ID tool wear and it is shown in Figure 4-9. Several interesting effects can be seen from this plot. When comparing the ID depth of cut with the spindle speed, it is evident that as the spindle speed is increased at lower depths of cut there is a greater increase in wear. This is due to the eccentricity

effect of the work piece. When comparing the OD depth of cut with the spindle speed, it can be seen that when the speed is at centerpoint levels the OD Depth of cut can be increased to any level and it will not affect the wear of the ID tool.

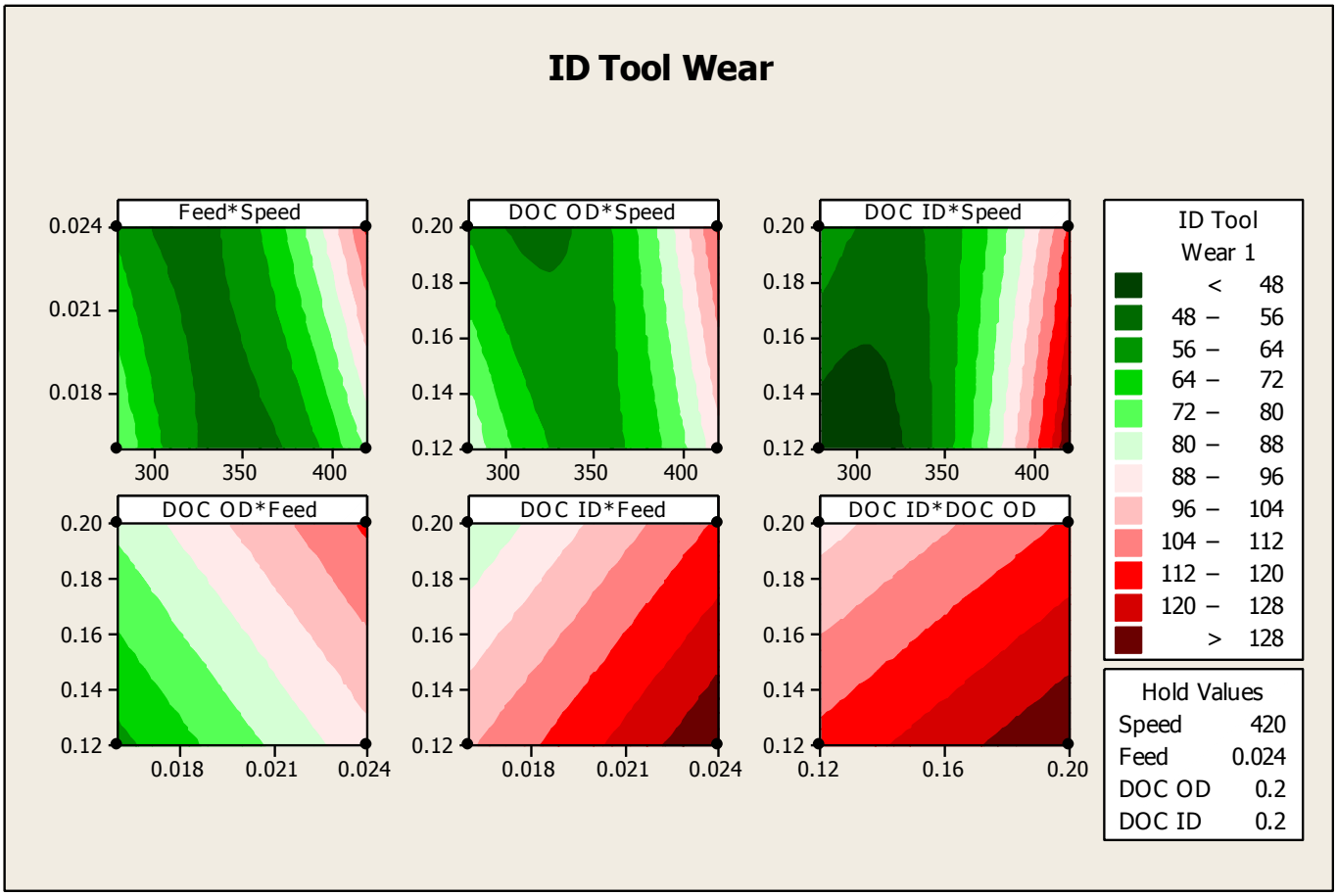

Figure 4-9: Contour Plots of the ID Tool Wear Model

The results from the ID tool wear model were compared from RSII to RSIII. The increase in wear of the tool is evident from RSII to RSIII. The model accuracy increased to an R-sq. value of 94.38% for RSIII indicating a clearer flank wear trend line on the tool edges. The comparison is shown in Table 4-18.

Table 4-18: Comparison of the ID Tool Wear Model between RSII and RSIII

Model Point	Spindle Speed (rpm)	Feed rate (in/rev)	OD DOC (in)	ID DOC (in)	RSII - ID Tool Wear (mm)	RSIII -ID Tool Wear (mm)	Percent increase (%)
1	325	0.018	0.150	0.170	59.032	68.907	14.330%
2	350	0.020	0.130	0.140	58.255	63.764	8.639%
3	375	0.023	0.170	0.190	68.082	85.198	20.089%

4.1.10 Cost Model

The cost model is the fundamental model to be used in the optimization of the simultaneous cutting operation as it is the driving factor for the Red Lion facility. The cost function was derived in section 2.4. The results from the analysis of variance of the cost function applied to RSII can be seen on Table 4-19.

Table 4-19: Analysis of Variance of the Cost Model

Source	D.O.F	Seq SS	Adj SS	Adj MS	F	P
Regression	5	0.539	0.539	0.108	126.750	0.000
Linear	2	0.188	0.188	0.094	110.520	0.000
Speed	1	0.043	0.043	0.043	50.350	0.000
Feed	1	0.145	0.145	0.145	170.700	0.000
Square	2	0.153	0.153	0.077	90.240	0.000
Speed*Speed	1	0.143	0.033	0.033	39.350	0.000
Feed*Feed	1	0.010	0.010	0.010	11.860	0.002
Interaction	1	0.197	0.197	0.197	232.240	0.000
Speed*Feed	1	0.197	0.197	0.197	232.240	0.000
Residual Error	25	0.021	0.021	0.001		
Lack-of-Fit	3	0.001	0.001	0.000	0.460	0.714
Pure Error	22	0.020	0.020	0.001		
Total	30	0.560				

The cost function model was a full second order model of the spindle speed and feed rate factors. Since the depths of cut were not considered in the tool life applications, this model was expected. The highest contributing factor to the cost is the combination of the spindle speed and feed rate terms. With the application of the cost function to the RSII model, the cost per test can be calculated with a R-Sq. value of 96.21% and a standard deviation of 0.0291579 $. The cost function applied to RSII yielded the equation in terms of the factors and it is shown in Equation 4.10.

$$\begin{aligned} Cost(\$) = {} & 9.13223 - 0.0226590 \times x_1 - 296.061 \times x_2 + 2.00394E\text{-}05 \times x_1^2 \\ & + 3368.84 \times x_{2_1}^2 + 0.396741 \times x_1 \times x_2 \end{aligned} \quad (4.10)$$

The response surface for the cost was plotted in Figure 4-10 to show the relationship between the spindle speed and the feed rate. From the plot it can be seen that a lower spindle speed and feed rate cause a high rise in costs due to the labor rate, but as the spindle speeds and feed rates are raised to high levels, the costs begin to rise due to the tool life .

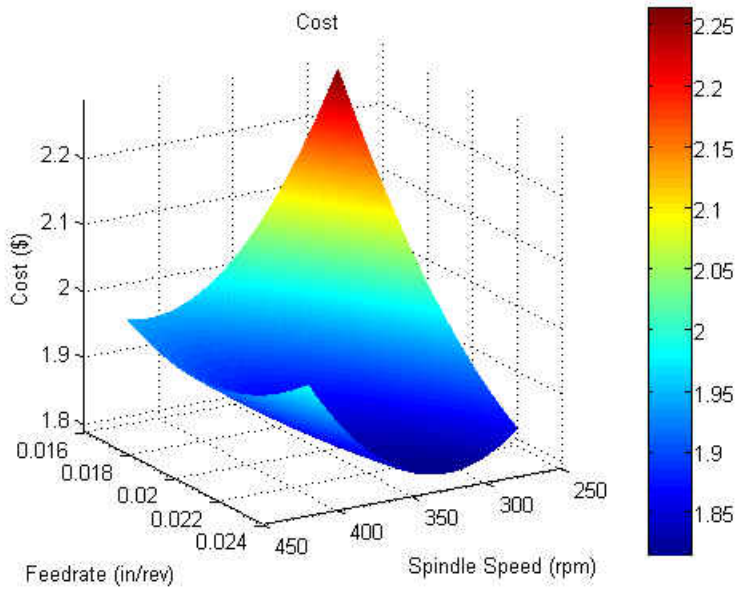

Figure 4-10: Surface Plot of the Cost Model

The cost model for RSII was compared to the cost of RSIII and the results are nearly the same. The only factor affecting the slight changes in the response is the cut time. Since there are slight differences in the cut time from RSII to RSIII there is a slight percent error shown in Table 4-20.

Table 4-20: Comparison of the Cost Model between RSII and RSIII

Model Point	**Spindle Speed (rpm)**	**Feed rate (in/rev)**	**OD DOC (in)**	**ID DOC (in)**	**RSII - Cost ($)**	**RSIII - Cost ($)**	**Percent Error (%)**
1	325	0.018	0.150	0.170	1.992	1.999	-0.356%
2	350	0.020	0.130	0.140	1.860	1.860	0.013%
3	375	0.023	0.170	0.190	1.845	1.846	-0.061%

4.2 Optimization

The optimization of the simultaneous cutting operation is focused on the Red Lion facility. In the previous sections the results show that the sensor signals along with other important factors such as the cut time, tool wear, and cost are modeled to represent the cutting operation using the four factors of spindle speed, feed rate, OD depth of cut and ID depth of cut based around Red Lion facility settings.

Most operations in the Red Lion facility require a heavy material removal pass followed by a finishing pass to machine the work pieces to specification and desired surface roughness. Two material removal operations and a finishing pass would be less of a toll on the lathe but would cost more money due to the labor rate of adding another pass. The heaviest material removal pass allowed by this research is 0.200 in both in the OD and the ID. Pushing the machine past these depths of cut would result power consumption greater than the lathe can output.

To compare how each one of the factors affects the responses an overlaid contour plot was created with all ten responses and it is shown in Figure 4-11. This plot holds the depths of cut constant at 0.200 in to allow for maximum material removal in the first pass. In the center of the overlaid contour plot one can see the settings used by the Red Lion facility.

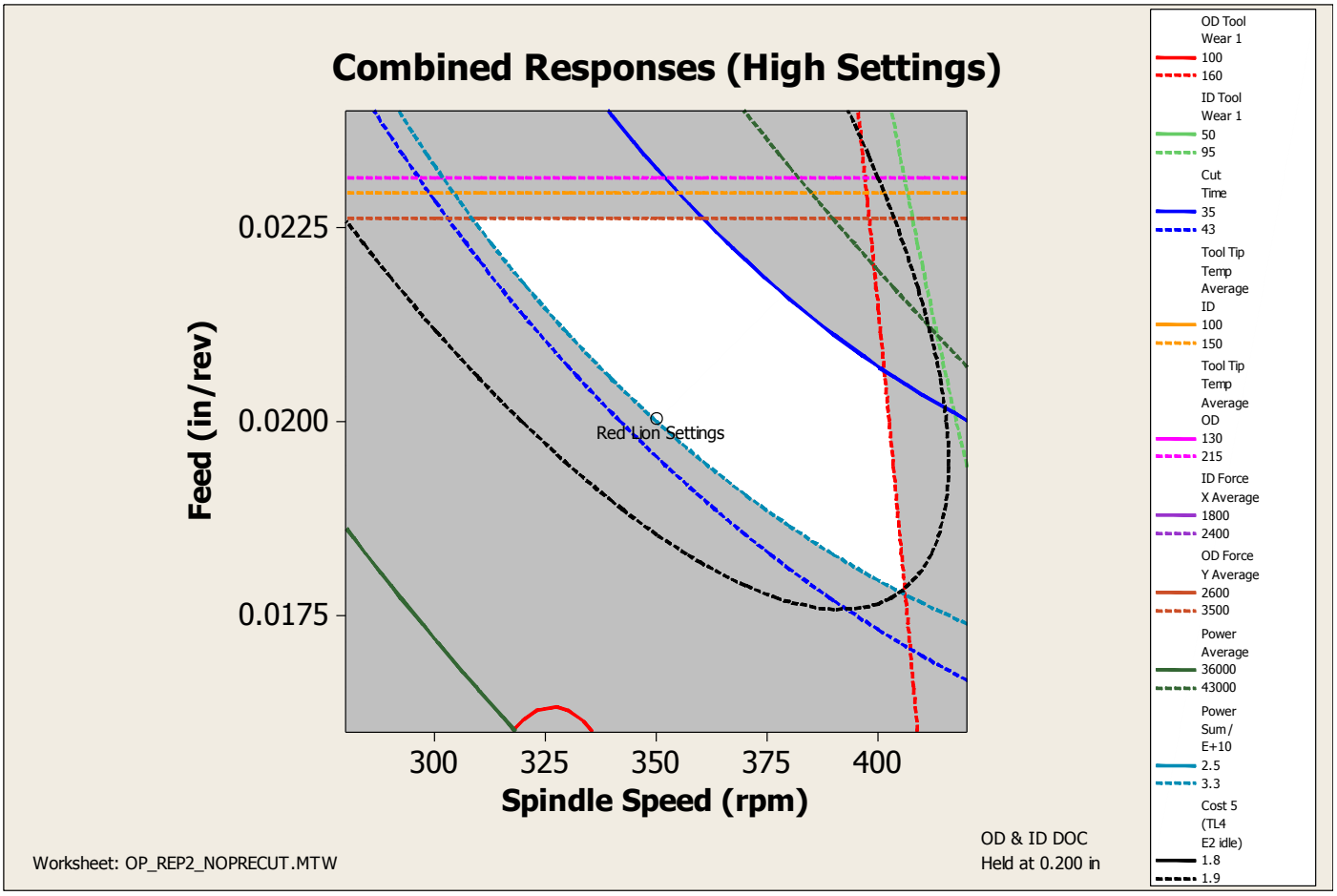

Figure 4-11: Contour Plot of Combined Responses at High Depths of Cut

From the overlaid contour plot the responses can be compared to decide on optimal operating levels. Since the forces and temperatures are generally functions of the feed rate and depths of cuts, they set the general limitation on the allowed feed rate. The cut time, average power, and sum of the power all show similar trends with increasing spindle speeds and feed rates. The goal of optimization is to reduce the cut time and the sum of power, while staying in an available operating range of the average power. To keep the lathe from operating at maximum power an operation condition of <43 kW was chosen. The overlaid contour plot also shows the

similarity of the effects of the spindle speed and feed rates on the OD and ID tool wear. The most important factor considered for the optimization is the cost which is represented by the dashed black line. Inside the black dashed line the cost is below $1.90.

Using the desirability function centered around cost minimization, the optimal settings for the Red Lion facility are a spindle speed of 365 rpm and a feed rate of 0.0223 holding the depths of cut constant at their highest settings. This can be seen in Minitab's Optimization Plot shown in Figure 4-12. The plot shows that both the OD and ID tool wear models are not at their minimal levels, but the cost is close to the minimum.

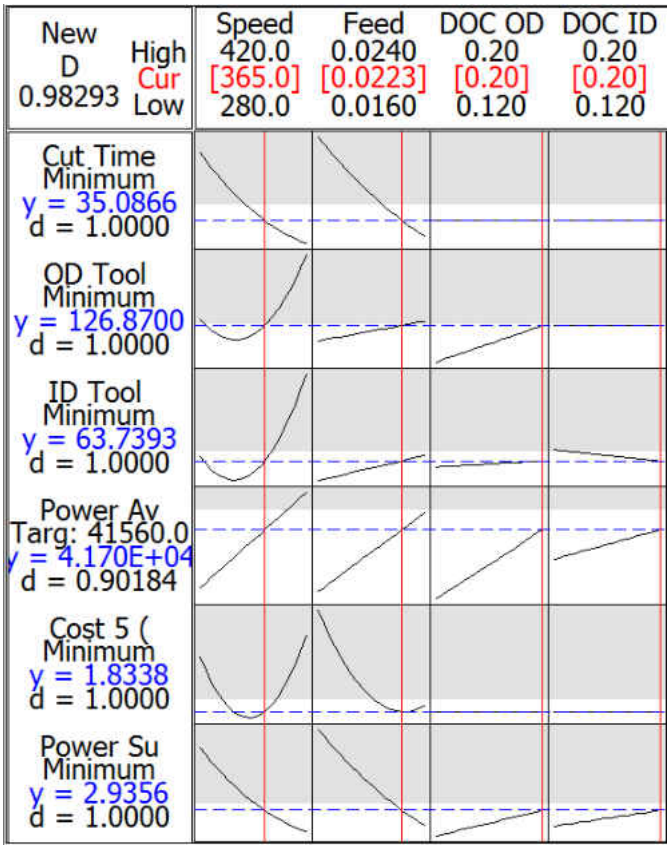

Figure 4-12: Response Optimizer

To compare the optimal settings to the Red Lion facility settings a table was created. In Table 4-21, it is seen that the optimization reduced the cost, sum of power, and the cut time. The tradeoff was a slight increase in average power and increases in both OD and ID tool wear. The cost decrease does not show the decreases in cost that the company could potentially save in overall power consumption. By reducing the overall power required to produce a work piece by over 12% the overall facility costs of electricity will be decreased.

Table 4-21: Comparison of Results between Red Lion and Proposed Optimum

Responses	**Units**	**Red Lion Settings**	**Proposed Optimum**	**% Difference**
OD Tool Wear	µm	113.54	126.87	10.51%
ID Tool Wear	µm	56.1934	63.7393	11.84%
Cut Time	s	41.7405	35.0866	-18.96%
Average Power	W	39652.1	41700	4.91%
Sum of Power	W/E+10	3.29228	2.9356	-12.15%
Cost	$	1.85899	1.8338	-1.37%

The results from the optimization have led to an improvement in productivity while still reducing cost. It is of importance to note that these results are valid for the given tool wear conditions. As the tool wears further, an expected increase of power will be seen along with increasing forces on the tool. A further study should be performed to determine how the empirical models will change throughout the entire life of the tool.

5 CHAPTER 5. CHAPTER 5 – CONCLUSION & FUTURE RESEARCH

The research presented in this paper focuses on the use of the Response Surface Method to build empirical models based off of the four process parameters chosen and to optimize the machining process. The results from the designs of experiments proved that cost reductions could be made while reducing the production time and power consumption. The next phase of the research project should allow for the implementation of the statistical results gathered to an adaptive controller.

Before construction of an adaptive controller is considered, correlation analysis must be made between the empirical models of each sensor signal. The multitude of sensors added to the lathe could prove costly once the price of the data acquisition equipment is also taken into account. Several of the sensor signals maybe reiterating each other so regression analysis may be performed to acquire one sensor response from another. By doing so, a limited amount of sensors that monitor the cutting operation can be carefully chosen. This will also limit the amount of data acquired thus limiting the amount of equipment required to acquire data.

Another area that could be investigated further is the tool life of the inner diameter boring tool. If a tool life model is designed for the inner diameter, then a simultaneous cost function could be derived. Since the outer diameter tool wear is much greater than the inner diameter tool wear, this is not required as the outer diameter tool will need replacement prior to the inner diameter tool.

The application of the Taylor Tool Life model for the outer diameter was one of the key results used in obtaining cost. Although the depth of cut does not have a large impact on the tool

life, several researchers have developed a Taylor Tool Life model using the cutting speed, feed rate and depth of cut. Due to the limited amount of work pieces used in this research the extra amount of data points required to include the depth of cut in the tool life model could not be achieved. The accuracy of the results could be increased by including the depth of cut in the model.

The design of experiments approach to find optimal settings proved useful in this manufacturing operation. A downfall of this method is that the empirical models derived for each sensor signal are only true to the region of tool life explored which is in the beginning phase. Several sensor signals such as force, power and sound change as the tool wear progresses thus changing the optimal region. To identify how the forces will change over the life of the tool, several design points could be experimented on until tool failure. The limited amount of work pieces did not allow for this testing to be performed.

APPENDIX A: RESPONSE SURFACE II RESULTS

Run	Cut Time	Average Power	Power Sum	OD Feed Force	ID Feed Force
1	67.636	32327.757	4.360	1257.109	2035.710
2	43.372	39875.555	3.459	2358.503	1968.211
3	64.227	33450.056	4.297	2419.100	1126.680
4	27.218	43153.098	2.349		1290.554
5	42.038	36879.678	3.101	2636.494	1631.967
6	43.568	38844.084	3.384	3579.060	2264.202
7	40.976	36753.636	3.012	2620.623	1611.359
8	45.271	33868.287	3.066	1644.865	1048.250
9	44.928	33466.651	3.007	2118.090	1212.306
10	28.750	39830.680	2.290	1993.446	2197.175
11	29.150	45284.649	2.640		2401.604
12	42.364	36478.047	3.091	2476.808	1640.688
13	46.450	37540.508	3.488	2722.469	1113.223
14	66.450	30958.738	4.114	1624.505	1191.925
15	65.847	34550.115	4.550	2716.598	1952.276
16	42.956	37241.733	3.200	3498.556	1238.590
17	27.564	37637.140	2.075	2295.138	1277.512
18	44.110	36882.869	3.254	2593.380	
19	44.650	35085.125	3.133	2069.534	2229.023
20	44.660	35538.726	3.174	1592.406	1900.851
21	41.501	37785.638	3.136	2530.156	2078.826
22	41.809	38528.305	3.222	3062.886	1607.138
23	52.374	34834.543	3.649	2394.293	1472.023
24	41.686	36683.503	3.058	2578.853	1559.475
25	34.565	39174.157	2.708	2617.112	1608.026
26	34.116	39100.114	2.668	2892.703	1808.953
27	41.788	34636.683	2.895	1910.695	1595.003
28	41.060	36713.787	3.015	2541.532	1665.598
29	41.717	35943.819	2.999	2654.641	1179.427
30	53.887	34597.327	3.700	2482.387	1684.808
31	41.592	36729.966	3.055	2606.162	1591.839

Run	OD Tool Temperature	ID Tool Temperature	OD Tool Wear	ID Tool Wear
1	134.252	144.979	89.493	101.167
2	172.373	155.756	171.205	89.493
3	148.097	117.356	128.404	77.820
4	192.023	126.407	202.333	155.641
5	191.856	125.242	77.820	58.365
6	240.362	166.627	128.404	73.929
7	194.515	113.899	97.276	89.493
8	125.817	108.296	147.859	97.276
9	147.678	107.143	112.840	46.692
10	161.652	152.293	151.750	77.820
11	218.846	153.019	241.243	120.622
12	197.956	123.242	73.929	42.801
13	199.332	115.422	155.641	81.711
14	130.248	106.946	112.840	93.385
15	207.333	122.463	108.949	58.365
16	241.393	119.392	140.077	42.801
17	141.327	123.187	132.295	116.731
18	172.490	123.571	128.404	
19	161.699	174.776	116.731	101.167
20	134.099	145.638	128.404	70.038
21	172.200	130.465	101.167	58.365
22	201.780	119.475	93.385	54.474
23	155.505	131.182	116.731	66.147
24	179.357	124.312	77.820	35.019
25	178.354	126.171	136.186	73.929
26	191.110	132.440	97.276	62.256
27	137.330	122.278	105.130	66.147
28	167.780	129.492	108.949	54.474
29	184.404	118.549	97.276	46.692
30	180.829	125.926	151.750	58.365
31	173.234	118.156	101.241	54.474

APPENDIX B: RESPONSE SURFACE III RESULTS

Run	Cut Time	Average Power	Power Sum	OD Feed Force	ID Feed Force
1	67.000	31091.849	4.166	1359.029	1152.254
2	28.030	37649.575	2.111	1805.479	1393.912
3	41.550	36568.424	3.039	2301.672	1707.569
4	65.400	34752.099	4.546	2561.062	2052.235
5	44.250	34955.677	3.094	1869.116	2412.995
6	41.500	36687.339	3.045	2329.209	1685.711
7	41.500	37938.768	3.149	2599.959	1194.494
8	43.225	36981.908	3.197	3326.610	1372.747
9	43.760	35968.501	3.148	1611.616	2061.730
10	29.150	45284.649	2.640	4327.202	2401.604
11	41.273	37051.475	3.058	2669.727	
12	67.597	31878.700	4.310	1463.608	2079.952
13	44.600	38839.904	3.465	3480.954	2297.610
14	43.970	33934.078	2.984	1688.193	1234.174
15	42.420	33403.327	2.834	2033.781	1340.858
16	27.829	42972.801	2.392	3842.338	1587.731
17	42.390	39711.915	3.367	2856.842	2037.826
18	66.632	33572.592	4.474	2696.569	1106.220
19	42.710	36918.170	3.154	2723.132	
20	29.956	39859.597	2.388	2003.429	2479.558
21	42.670	37063.684	3.163	2565.661	1637.504
22	42.352	36041.408	3.053	2592.260	1193.004
23	41.028	37037.318	3.039	2660.516	1663.453
24	34.310	38972.436	2.674	2801.387	1898.011
25	41.658	37360.619	3.113	2513.487	2128.896
26	52.156	34572.121	3.606	2401.494	1711.168
27	51.946	34604.340	3.595	2223.886	1499.766
28	41.592	38476.706	3.201	3095.504	1673.089
29	34.071	39613.292	2.699	2741.791	1677.367
30	42.274	34940.198	2.954	1837.405	1717.858

Run	OD Tool Temperature	ID Tool Temperature	OD Tool Wear	ID Tool Wear
1	150.834	102.273	93.385	97.276
2	150.598	129.992	186.789	105.058
3	182.401	138.620		66.147
4	194.498	119.207	112.840	70.038
5	152.211	149.697	97.276	101.167
6	178.449	133.082	105.058	62.256
7	196.738	113.030	175.096	58.365
8	208.455	114.241	190.660	77.820
9	134.141	141.162	140.077	89.493
10	218.846	153.019	338.519	128.404
11	184.498	126.749	143.968	
12	136.373	134.395	97.276	100.529
13	201.119	138.673	159.532	89.493
14	143.274	108.824	147.859	97.276
15	159.793	116.261	105.058	73.929
16	203.392	117.447	319.064	105.058
17	189.521	126.379	198.442	70.038
18	194.655	102.671	124.513	85.602
19	179.265	113.365	155.641	
20	153.286	140.075	147.859	
21	191.326	116.765	120.622	62.256
22	179.596	117.743	120.622	54.474
23	181.444	114.389	128.404	62.256
24	179.363	128.027	132.295	81.711
25	177.359	150.094	116.731	70.038
26	190.927	121.150	143.968	70.038
27	159.256	123.605	136.186	77.820
28	192.676	134.510	159.532	54.474
29	178.054	139.357	178.987	73.929
30	147.598	128.628	128.404	62.256

LIST OF REFERENCES

1. Myers, R., D. Montgomery, and C. Anderson-Cook, *Response Surface Methodology: Process and Product Optimization Using Designed Experiments*. Third Edition ed. Wiley Series in Probability and Statistics. 2009, Hoboken: Wiley. 680.
2. O'Donnell, G., et al., *Towards the improvement of tool condition monitoring systems in the manufacturing environment.* Journal of Materials Processing Technology, 2001. **119**(Compendex): p. 133-139.
3. Sharma, V.S., M. Dogra, and N.M. Suri, *Advances in the turning process for productivity improvement - a review.* Proceedings of the Institution of Mechanical Engineers, Part B (Journal of Engineering Manufacture), 2008. **222**(Copyright 2009, The Institution of Engineering and Technology): p. 1417-42.
4. Srinivas, J., R. Giri, and Y. Seung-Han, *Optimization of multi-pass turning using particle swarm intelligence.* International Journal of Advanced Manufacturing Technology, 2009. **40**(Copyright 2010, The Institution of Engineering and Technology): p. 56-66.
5. Rao, B.C. and Y.C. Shin, *Comprehensive dynamic cutting force model for chatter prediction in turning.* International Journal of Machine Tools and Manufacture, 1999. **39**(Compendex): p. 1631-1654.
6. Tlusty, J., *Manufacturing Processes and Equipment*. 1 ed. 1999, Upper Saddle River: Prentics Hall. 928.
7. Kuljanic, E., G. Totis, and M. Sortino, *Development of an intelligent multisensor chatter detection system in milling.* Mechanical Systems and Signal Processing, 2009. **23**(Copyright 2009, The Institution of Engineering and Technology): p. 1704-18.

8. Bouacha, K., et al., *Statistical analysis of surface roughness and cutting forces using response surface methodology in hard turning of AISI 52100 bearing steel with CBN tool.* International Journal of Refractory Metals and Hard Materials, 2010. **28**(Compendex): p. 349-361.

9. Kuljanic, E., M. Sortino, and G. Totis, *Multisensor approaches for chatter detection in milling.* Journal of Sound and Vibration, 2008. **312**(Copyright 2008, The Institution of Engineering and Technology): p. 672-93.

10. Kwak, J.-S., S.-B. Sim, and Y.-D. Jeong, *An analysis of grinding power and surface roughness in external cylindrical grinding of hardened SCM440 steel using the response surface method.* International Journal of Machine Tools and Manufacture, 2006. **46**(Compendex): p. 304-312.

11. Kang-Ning, L. and L. Cheng-Jen, *An intelligent sensor fusion system for tool monitoring on a machining centre.* International Journal of Advanced Manufacturing Technology, 1997. **13**(Copyright 1997, IEE): p. 556-65.

12. Palanikumar, K. and R. Karthikeyan, *Optimal machining conditions for turning of particulate metal matrix composites using Taguchi and response surface methodologies.* Machining Science and Technology, 2006. **10**(Compendex): p. 417-433.

13. Dongfeng, S. and N.N. Gindy, *Development of an online machining process monitoring system: Application in hard turning.* Sensors and Actuators A (Physical), 2007. **135**(Copyright 2007, The Institution of Engineering and Technology): p. 405-14.

14. Chua, M.S., et al., *Determination of optimal cutting conditions using design of experiments and optimization techniques.* International Journal of Machine Tools and Manufacture, 1993. **33**(Compendex): p. 297-305.

15. Yang, W.H. and Y.S. Tarng, *Design optimization of cutting parameters for turning operations based on the Taguchi method.* Journal of Materials Processing Technology, 1998. **84**(Compendex): p. 122-129.

16. Kirby, D., Z. Zhang, and J. Chen, *Development of an Accelerometer-Based Surface Roughness Prediction System in Turning Operations Using Multiple Regression Techniques.* Journal of Industrial Technology, 2004. **20**(4).

17. Choudhury, I.A. and M.A. El-Baradie, *Machinability assessment of inconel 718 by factorial design of experiment coupled with response surface methodology.* Journal of Materials Processing Technology, 1999. **95**(Compendex): p. 30-39.

18. Geng, H., *Manufacturing Engineering Handbook*. 2004, New York: McGraw-Hill.

19. Kopac, J. and S. ali. *Tool wear monitoring during the turning process*. in *5th Asia Pacific Conference on Materials Processing, June 25, 2001 - June 25, 2001*. 2001. Seoul, Korea, Republic of: Elsevier Ltd.

20. Choudhury, S.K. and K.K. Kishore, *Tool wear measurement in turning using force ratio.* International Journal of Machine Tools and Manufacture, 2000. **40**(Compendex): p. 899-909.

21. Li, X., *A brief review: Acoustic emission method for tool wear monitoring during turning.* International Journal of Machine Tools and Manufacture, 2002. **42**(Compendex): p. 157-165.

22. Moriwaki, T. and M. Tobito. *New approach to automatic detection of life of coated tool based on acoustic emission measurement*. in *Sensors and Controls for Manufacturing - 1988, November 27, 1988 - December 2, 1988*. 1988. Chicago, MI, USA: Publ by American Soc of Mechanical Engineers (ASME).

23. Govekar, E., J. Gradisek, and I. Grabec. *Analysis of acoustic emission signals and monitoring of machining processes*. in *Ultrasonics International 1999 Joint with 1999 World Congress on Ultrasonics, 29 June-1 July 1999*. 2000. Netherlands: Elsevier.

24. Kurada, S. and C. Bradley, *A review of machine vision sensors for tool condition monitoring.* Computers in Industry, 1997. **34**(Copyright 1997, IEE): p. 55-72.

25. Amaitik, S.M., T.T. Tasgin, and S.E. Kilic, *Tool-life modelling of carbide and ceramic cutting tools using multi-linear regression analysis.* Proceedings of the Institution of Mechanical Engineers, Part B (Journal of Engineering Manufacture), 2006. **220**(Copyright 2006, The Institution of Engineering and Technology): p. 129-36.

26. Malstrom, E.M., *What every engineer should know about manufacturing cost estimating.* . 1981, New York: Marcel Dekker. 181.

27. Khuri, A. and J. Cornell, *Response Surfaces Designs and Analyses*. 2 ed. STATISTICS: Textbooks and Monographs, ed. D.B. Owen. 1996, New York: Marcel Dekker. 510.